AD-A090 536 SCIENCE APPLICATIONS INC CANOGA PARK CA COMBUSTION D--ETC F/G 21/5
MIXING AND COMBUSTION IN HIGH SPEED AIR FLOWS.(U)
JUL 80 P T HARSHA, R B EDELMAN F49620-77-C-0044
UNCLASSIFIED SAI-80-020-CP AFOSR-TR-80-1005 NL

END
DATE FILMED
11-80
DTIC

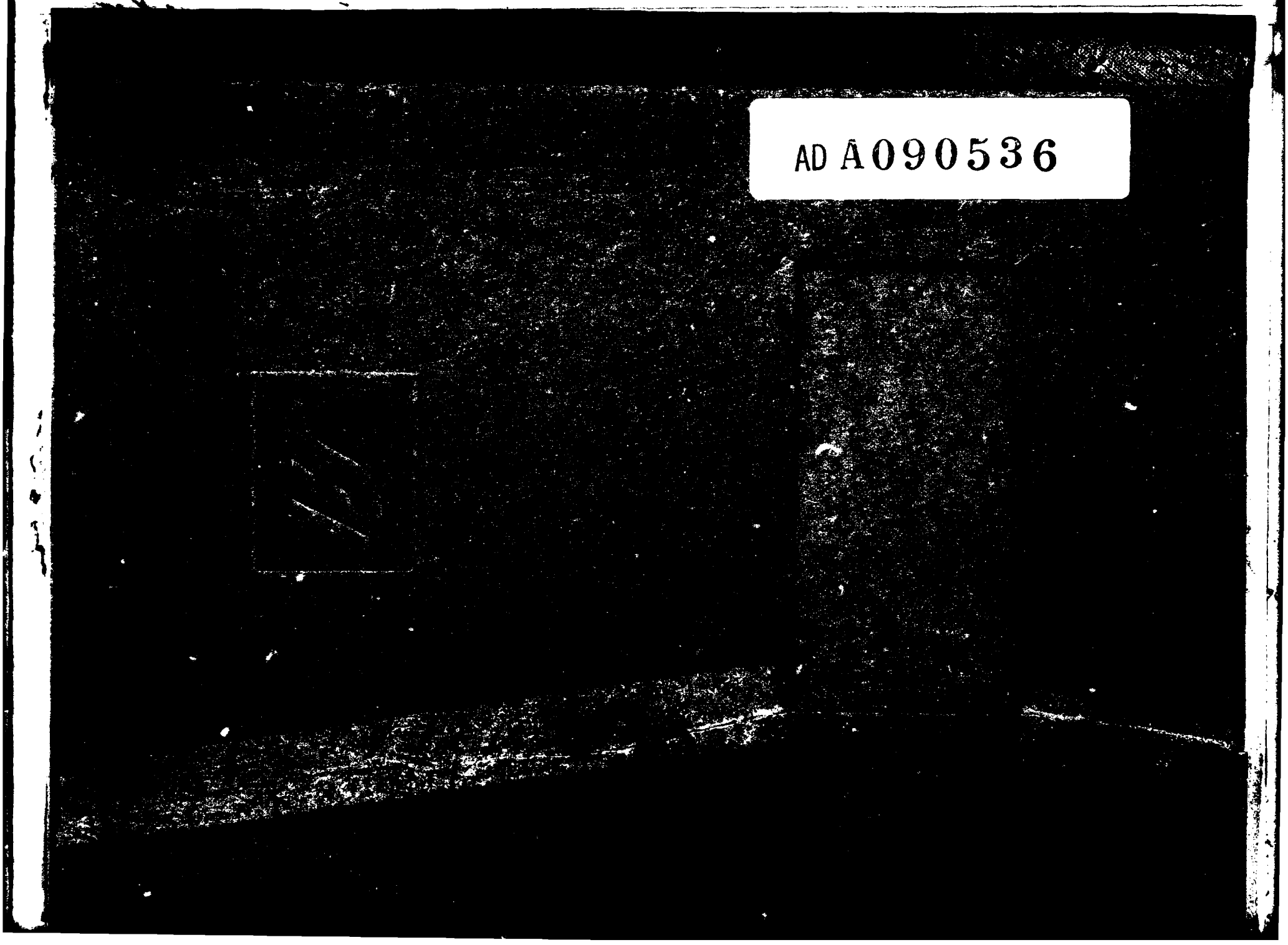
AD A090536

SAI-80-020-CP

MIXING AND COMBUSTION

IN

HIGH SPEED AIR FLOWS

Final Report for Period April 1977 - May 1980

Under Contract No. F49620-77-C-0044

DTIC
ELECTE
OCT 17 1980
S
C

P. T. Harsha and R. B. Edelman

Science Applications, Inc.
Combustion Dynamics and Propulsion Technology Division
21133 Victory Boulevard, Suite 216
Canoga Park, California 91303

Prepared for

Air Force Office of Scientific Research
Bolling Air Force Base
Washington, D.C. 20332

July 1980

Approved for public release; distribution unlimited.

AIR 7

Qualified requestors may obtain additional copies from the Defense Documentation Center, all others should apply to the National Technical Information Service.

Conditions of Reproduction

Reproduction, translation, publication, use and disposal in whole or in part by or for the United States Government is permitted.

AIR FORCE OFFICE OF SCIENTIFIC RESEARCH (AFSC)
NOTICE OF TRANSMITTAL TO DDC
This technical report has been reviewed and is approved for public release IAW AFR 190-12 (7b).
Distribution is unlimited.
A. D. BLOSE
Technical Information Officer

Unclassified

SECURITY CLASSIFICATION OF THIS PAGE (When Data Entered)

REPORT DOCUMENTATION PAGE	READ INSTRUCTIONS BEFORE COMPLETING FORM
1. REPORT NUMBER: AFOSR-TR-80-1005	2. GOVT ACCESSION NO.: AD-A090536
	3. RECIPIENT'S CATALOG NUMBER:
4. TITLE (and Subtitle): MIXING AND COMBUSTION IN HIGH SPEED AIR FLOWS	5. TYPE OF REPORT & PERIOD COVERED: Final, April 1977 — May 1980
	6. PERFORMING ORG. REPORT NUMBER: SAI-80-020-CP
7. AUTHOR(s): P. T. Harsha, R. B. Edelman	8. CONTRACT OR GRANT NUMBER(s): F49620-77-C-0044
9. PERFORMING ORGANIZATION NAME AND ADDRESS: SCIENCE APPLICATIONS, INC, 21133 Victory Blvd., Suite 216, Canoga Park, California 91303	10. PROGRAM ELEMENT, PROJECT, TASK AREA & WORK UNIT NUMBERS: 2308/A2, 61102F
11. CONTROLLING OFFICE NAME AND ADDRESS: Air Force Office of Scientific Research/NA, Bldg. 410, Bolling Air Force Base, D.C. 20332	12. REPORT DATE: July 1980
	13. NUMBER OF PAGES: viii + 56
14. MONITORING AGENCY NAME & ADDRESS (If different from Controlling Office)	15. SECURITY CLASS. (of this report): Unclassified
	15a. DECLASSIFICATION/DOWNGRADING SCHEDULE

16. DISTRIBUTION STATEMENT (of this Report)

Approved for public release; distribution unlimited.

17. DISTRIBUTION STATEMENT (of the abstract entered in Block 20, if different from Report)

18. SUPPLEMENTARY NOTES

19. KEY WORDS (Continue on reverse side if necessary and identify by block number)

Sudden expansion (dump) burner.
Integral rocket/ramjet engine.
Recirculating reacting high-speed flows.
Modeling sudden-expansion combustor flowfield.

20. ABSTRACT (Continue on reverse side if necessary and identify by block number)

The development and application of a modular model for the prediction of the performance of sudden expansion burners as a function of the controllable parameters relevant to combustor design is described. The model is based on a concept in which the recirculation zone, treated as a stirred reactor, is coupled to a parabolic boundary layer formulation for the flow outside the recirculation zone. Hydrocarbon oxidation kinetics and turbulent kinetic energy models are employed in the model development. In addition to the parabolic-flow and stirred reactor →

DD FORM 1 JAN 73 1473 EDITION OF 1 NOV 65 IS OBSOLETE

Unclassified

SECURITY CLASSIFICATION OF THIS PAGE (When Data Entered)

411 174

elements, a module representing the fuel injection process has been developed. Results of the application of the modular model to the analysis of cold-flow and reacting-flow dump combustor experimental data are described.

SUMMARY

A modular model of the sudden-expansion combustor has been developed and applied to the computation of a variety of sudden-expansion flowfields, both reacting and non-reacting. The modular concept involves the representation of a complex flowfield through the use of detailed models of flowfield regions, coupled together through their boundary conditions. For the sudden-expansion combustor, basic elements of the model include a parabolic directed-flow computation and a well-stirred reactor model representing the recirculation region(s). The parabolic module incorporates a two-equation turbulent kinetic energy turbulence model, and both the directed flow and stirred reactor elements make use of the quasiglobal formulation for the treatment of finite-rate hydrocarbon chemical kinetics. Coupling between the modules is through a shear layer representation which provides the parabolic-flow boundary conditions and the stirred reactor feed rates. Compared to unified elliptic models of the dump combustor, the major advantage of this approach is the greatly increased detail possible in the combustor analysis. This detail in turn allows the development of chemical kinetic and flowfield models applicable to the refinement of elliptic formulations.

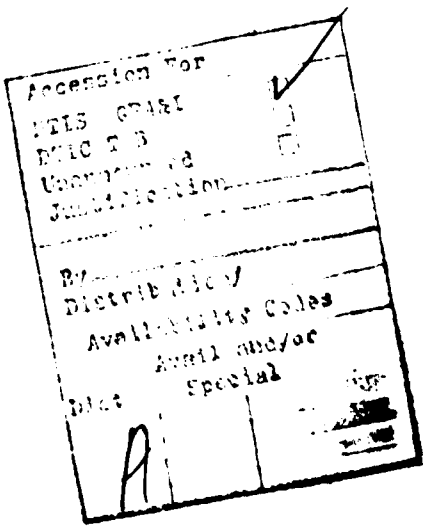

ABSTRACT

The development and application of a modular model for the prediction of the performance of sudden-expansion burners as a function of the controllable parameters relevant to combustor design is described. The model is based on a concept in which the recirculation zone, treated as a stirred reactor, is coupled to a parabolic boundary layer formulation for the flow outside the recirculation zone. Hydrocarbon oxidation kinetics and turbulent kinetic energy models are employed in the model development. In addition to the parabolic-flow and stirred reactor elements, a module representing the fuel injection process has been developed. Results of the application of the modular model to the analysis of cold-flow and reacting-flow dump combustor experimental data are described.

TABLE OF CONTENTS

LIST OF FIGURES

LIST OF FIGURES (continued)

LIST OF TABLES

NOMENCLATURE

Latin Symbols

a	coefficient in shear layer width expression, Eq. 29
b	coefficient in shear layer width expression, Eq. 29 mixing region width, Eq. 13
c	viscosity model coefficient, Eq. 13
C_{FW}	effective "skin friction" coefficient, dividing streamline
C_{E1}	two-equation turbulence model coefficient, = 1.40
C_{E2}	two-equation turbulence model coefficient, = 1.95
C_{μ}	two-equation turbulence model coefficient, = 0.09
d	diffusion coefficient in stirred reactor/directed flow coupling condition, Eq. 35 - 37 drop diameter, Eq. 44
d_0	initial drop diameter, Eq. 44
h	static enthalpy combustor dump step height
h^I	enthalpy influx to well-stirred reactor
H	total enthalpy
k	turbulent kinetic energy
ℓ	shear layer width
ℓ_k	turbulent kinetic energy dissipation rate length scale
L	recirculation zone length
$\dot{m}$	well-stirred reactor flow rate
$\dot{m}^I$	flow rate into well-stirred reactor
$\dot{m}^O$	flow rate out of well-stirred reactor
M	mass resident in well-stirred reactor
$\dot{n}_A$	volumetric air flow rate into well-stirred reactor
Nu	Nusselt number
p	pressure
Pr	turbulent Prandtl number
$\dot{Q}$	heat input to well-stirred reactor

r	radial coordinate
R	gas constant
R_c	dividing streamline radius
Sc	turbulent Schmidt number
t	time
T	static temperature
T_i	initial temperature
T_o	total temperature
u	axial velocity component
v	radial velocity component
V	stirred reactor volume
$\dot{w}_i$	chemical production rate, species i
W_i	molecular weight, species i
x	axial coordinate

Greek Symbols

α_i	mass fraction of species i
α_v	vapor phase fuel mass fraction
ε	turbulent kinetic energy dissipation rate
η_C	temperature rise combustion efficiency
η_{ISP}	specific impulse combustion efficiency
κ	thermal conductivity
λ	droplet vaporization rate constant
μ_T	turbulent viscosity
ν_T	turbulent diffusivity
ρ	density
ρ_c	well-stirred reactor characteristic density
σ_k	turbulent kinetic energy exchange coefficient
σ_ε	turbulent kinetic energy dissipation rate exchange coefficient
τ_w	dividing streamline shear stress
ψ	*stream function:* for axisymmetric flow, at constant x: $\psi d\psi = \rho u r dr$

Subscripts

p	streamline outside recirculation region
r	"streamline" within recirculation region
R	well-stirred reactor value
w	dividing streamline value

SECTION 1 - INTRODUCTION

Control of flame stabilization and flame propagation in a turbulent flow represents a key element in combustion chamber design. The placement and geometry of fuel injectors, flameholders, and air distribution ports are basic design parameters that govern the performance of a particular combustor. Therefore it is desirable to compute combustion chamber flowfields in order to understand the phenomena that occur in existing combustors and to predict the performance of new combustor design concepts. In addition to the overall combustor flowfield, modeling can also be used to provide insight into the behavior of portions of the combustor, such as flameholders and fuel injectors, under a variety of conditions. The insight gained through the use of these "unit" analyses can be of substantial use in the planning of a combustor test program and in the interpretation of combustor and combustor component test data.

The computation of a generalized combustor flowfield is a formidable task, involving a number of complex, coupled physical and chemical processes, which can include turbulent, recirculating flow, possibly with swirl, finite-rate chemical kinetics, and droplet evaporation and combustion. The obvious difficulties include not only sorting out the multitude of coupled mechanisms but also involve the typical disparity in characteristic length and time scales in combustion chamber flows. Despite the problems involved, considerable progress has been made in recent years in the development of calculation methods for these flows, using techniques for the solution of the elliptic governing equations and simpler yet physically perceptive "modular" modeling techniques.

A "unified" model of an overall combustion chamber flowfield in general requires the numerical solution of the elliptic form of the governing equations, since most practical combustion chamber flows involve large regions of recirculation, in which axial diffusion is

important. A considerable amount of research effort has been put into the development of numerical techniques for these problems, and successful comparison of calculation with experiment for recirculating flows with large heat release has been reported by Hutchinson, et al. [1] and by Abou Ellail, et al. [2], for example. Significantly, in both cases a careful adaptation of the numerical model to the specific experimental configuration was reported to be required, and in both of these papers it was noted that the details of the computation required careful handling to obtain the accuracy demonstrated. Furthermore, Abou Ellail, et al. [2] note that it is not possible to provide sufficient resolution in a detailed combustor flowfield computation to adequately describe processes such as fuel injection for which the mixing process initially occurs on a scale much smaller than that of the overall combustion chamber.

Thus, while the development of numerical models capable of providing direct solution of the equations governing specific combustion chamber flowfields continues, a need exists for the development of physically perceptive yet mathematically simpler models. This requirement arises from both the need to provide a model which allows reasonably rapid computation of a number of different, complex combustor geometries, and the need to develop models for those processes, such as fuel injection, which occur on scales smaller than can be adequately resolved in a detailed overall flowfield computation. The development of approximate methods - modular models - is a response to the requirements just outlined.

The basic interest in the application of approximate techniques is to avoid the complexities inherent in a direct calculation of an elliptic flowfield by making suitable assumptions that allow the flow to be computed using simpler approaches. Clearly the simplest possible procedure is to assume that the flowfield is effectively one-dimensional thus avoiding any necessity for definition or calculation of velocity or species profile effects. A somewhat more sophisticated approach is to assume that the combustor flowfield can be broken down into separate zones, each of which can be calculated individually in some detail, and

then coupled together in some fashion to obtain an overall computational analog of the combustor flow. Such approaches are termed modular models, examples of which have been reported by Roberts, et al. [3] and Swithenbank, et al. [4]; the formulation described in this report, while similar to those of Roberts, et al. and Swithenbank, et al. in that the overall combustor flowfield is broken down into computational subunits, provides far more detail than either of the former models.

The sub-models used for the flowfield regions and the assumptions involved in the model formulations in each of the approaches described in references 3 and 4 have been discussed by Harsha and Edelman [5]. In the present approach, the combustor flowfield, represented schematically in Figure 1, is broken down into three major components: a directed flow, which is treated as parabolic, a recirculation zone, assumed to be represented by well-stirred reactor(s), and a turbulent shear layer along the dividing streamline which separates the other two regions. The shear layer serves as the coupling region between the other two model components; fluxes of species and energy across this shear layer form the boundary conditions on the two computational regions. Finite-rate chemistry, based on the quasiglobal model [6] is included in the formulations for both the directed flow and well-stirred reactor regions, although for the modular model calculations described in this report, the recirculation region well-stirred reactor formulation has been restricted to a global finite-rate chemistry model. The directed flow is assumed to be fully turbulent, with the turbulent viscosity defined by a two-equation turbulence model [7].

A key difference between this modular model and the models of Roberts, et al. [3] and Swithenbank, et al. [4] is the provision for the shear layer coupling region in the current model. Through the use of this element of the model, the division of the mass flux between the directed flow and the recirculation region is computed iteratively rather than specified empirically. Furthermore, the directed flow region is computed in detail as a two-dimensional parabolic flowfield, rather than through a one-dimensional approximation, allowing the use of detailed computations of the mixing and chemical reactions in this region of the combustor.

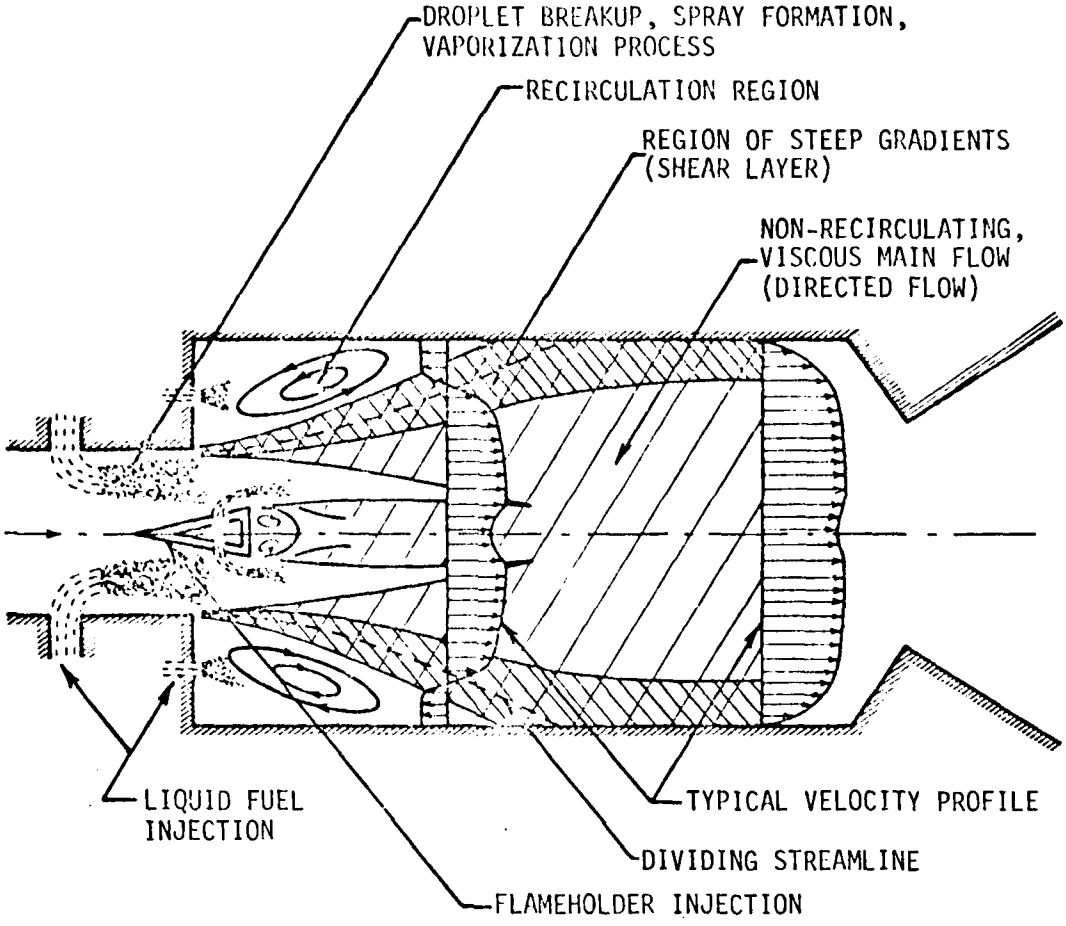

Figure 1. SCHEMATIC OF SUDDEN-EXPANSION (DUMP) BURNER

The features of the three modular models discussed in this section are summarized in Table 1. Although the present model is computationally more complex than the models of Roberts, et al. [3] and Swithenbank, et al. [4], and requires an iterative solution, the additional complexity allows the development of an overall combustor flowfield computation which can include far more detailed modeling than is possible with either of these approaches. Furthermore, each element of the present modular model - the well-stirred reactor, the parabolic flow computation, and the shear layer representation can be systematically

developed. For example, the effects of unmixedness can be introduced into both the stirred reactor module and the parabolic directed flow computation. Multiple well-stirred reactors can also be easily introduced for more detailed modeling of the recirculation region. The detail available in the parabolic flowfield computation allows the inclusion of models for processes such as liquid fuel injection, and the spread and vaporization of the resulting spray, treated either in bulk or through the use of detailed spray modeling. Thus, modular modeling of the type described in this report offers considerable potential for systematic development in complexity with the prospect of providing computational capabilities substantially equivalent to those available from direct solution of the elliptic equations, while at the same time providing greater insight into the physical details involved in a generalized combustor flowfield.

Table 1. COMPARISON OF MODULAR MODELS

	Roberts, et al. [3]	Swithenbank, et al. [4]	Present Model
Elements	Plug Flow Reactors	Plug Flow/Perfectly Stirred Reactors	Parabolic Flow/Stirred Reactors
Coupling Conditions	Empirical Flow Division	Empirical Flow Division	Iterative Solution For Flow Division
Turbulent Flow Characterization	None	None - Enters Empirical Flow Division	Turbulent Kinetic Energy Model
Chemistry Model	Quasiglobal H/C Kinetics	Global H/C Kinetics	Quasiglobal H/C Kinetics

In this report, the development of the modular model for a sudden-expansion combustor is described in detail. The model formulation, including the definition of coupling conditions and a description of the overall flowfield iteration procedure, is described in Section 2. Results of the application of the approach to the computation of a variety of sudden-expansion flowfields are described in Section 3; where the capabilities of this approach and current unified elliptic formulations overlap, such as in the computation of incompressible sudden-expansion flows, the results of the modular approach are compared with both available experimental data and unified model computational results.

As noted earlier, the analysis of combustor processes can make use of unit models as well as the overall modular technique. These unit models can then in turn provide elements of the modular approach, as well as providing insight into combustor design problems on their own. Examples of the application of unit process modeling are discussed in Section 4: these examples include the use of a simple fuel droplet vaporization model to interpret liquid spray combustion efficiency results and the use of the well-stirred reactor formulation to analyze flameholder blowout problems and to extend the range of available blowout correlations into regions applicable to ramjet development programs.

Overall conclusions reached from this work with regard to the problems of combustor modeling are discussed in Section 5. The work described in this report shows that there are considerable advantages to be gained from the use of analytical models as interpretative techniques and planning guides in conjunction with experimental combustor development programs, such as the coordination between this work and the experimental work at the Air Force Aeropropulsion Laboratories which has been maintained throughout the effort described herein.

SECTION 2 - MODULAR MODEL FORMULATION

The basic elements of the current modular model formulation are the parabolic finite-difference computational technique developed by Boccio, Weilerstein and Edelman [8], modified to incorporate the two-equation turbulent kinetic energy model developed by Launder, et al. [7], used for the directed-flow portion of the analysis, and the stirred reactor computation developed by Edelman and Weilerstein [9]. Both of these elements make use of the quasiglobal model developed by Edelman and Fortune [6] for rapid computation of finite-rate hydrocarbon air kinetics. These elements, or modules, are coupled together through a simplified representation of the turbulent shear layer which exists between the directed flow and the recirculation region. In the modular approach, the shear layer representation is used to define the gradients in velocity, species, and enthalpy between the two regions of the flow, thus providing both the boundary conditions on the directed flow and the stirred reactor feed rates. Details of the mathematical formulations used for the flowfield regions are discussed in this section; details of the numerical analysis procedure may be found in Appendix I.

2.1 WELL-STIRRED REACTOR - THE RECIRCULATION ZONE MODEL

Flowfield regions in which intense backmixing occurs can approach the limit of complete mixing, and thus the well-stirred reactor concept is attractive for representing the recirculation region(s) in a sudden-expansion burner. For a well-stirred reactor, the equations describing the transport of energy and species reduce to the relations

Continuity

$$\dot{m}^I = \dot{m}^O = \dot{m} \qquad (1)$$

Species

$$\frac{dM\alpha_i}{dt} = \dot{m}_i^I + V\dot{w}_i \tag{2}$$

Energy

$$h = \sum_i h_i \alpha_i = h^I + \dot{Q}/\dot{m} \tag{3}$$

where the superscripts I and O represent inflow to and outflow from the stirred reactor, M the mass contained within the stirred reactor, α_i are the mass fractions of the i species in the reactor, $\dot{m}_i^I$ the net inflow of species i, V is the reactor volume, $\dot{w}_i$ the volumetric production rate for species i due to chemical reaction, h the enthalpy, and $\dot{Q}$ the rate of heat addition to the reactor from its surroundings.

Note that in this set of equations the species transport equation is written in non-steady form. This formulation has been adopted to facilitate solution of the stirred reactor governing equations with finite-rate chemical kinetics; the steady-state stirred reactor solution is obtained when

$$\frac{d\alpha_i}{dt} = 0 \tag{4}$$

These equations, along with expressions for the volumetric production rates appearing in Eq. 2, expressions for the enthalpy as a function of species concentrations, and the equation of state, define the temperature and species concentrations in the stirred reactor, given the inflow rates for species and enthalpy. In the modular model, the net inflow of species and enthalpy can be expressed as line integrals involving gradients evaluated along the dividing streamline, so that for the modular model the energy and species conservation equations for the stirred reactor can be written

Energy

$$-2\pi\int_0^s R_c(x)\rho\nu_T\sum\left[h_i^I(T^I)\frac{\partial\alpha_i^I}{\partial r}\right]ds + \dot{Q} - 2\pi\int_0^s R_c(x)\kappa\frac{\partial T}{\partial s}ds =$$

$$2\pi\int_0^s R_c(x)\rho\nu_T\sum_i\left[h_i^0(T_R)\frac{\partial\alpha_i^0}{\partial r}\right]ds \qquad (5)$$

where $R_c(x)$ represents the radial location of the dividing streamline, and

Species

$$\frac{d\alpha_i}{dt} = \frac{-2\pi}{\rho_c V}\int_0^s R_c(x)\left[\rho\nu_T\frac{\partial\alpha_i^I}{\partial r}\right]ds - \frac{2\pi}{\rho_c V}\int_0^s R_c(x)\left[\rho\nu_T\frac{\partial\alpha_i^0}{\partial r}\right]ds + \frac{\dot{w}_i}{\rho_c} \qquad (6)$$

Here the superscript I refers to inflow into the stirred reactor (recirculation region) and superscript 0 refers to outflow from the stirred reactor, V is the reactor volume, ρ_c a characteristic density of the stirred reactor region, and $\rho\nu_T$ a characteristic eddy diffusivity, evaluated from the outer flowfield solution in the region of the dividing streamline. The term $\dot{w}_i$ represents the rate of production of species i caused by chemical reactions and $\dot{Q}$ represents the heat input to the stirred reactor region through the combustor walls.

2.2 PARABOLIC MIXING: THE DIRECTED-FLOW MODEL

The second major element of the modular model for a sudden-expansion combustor is the formulation for the directed flow portion of the combustor flowfield. It is assumed that the boundary layer approximations apply to this part of the flowfield, so that the describing equations are parabolic. For a steady, axisymmetric flow these equations may be written:

Global Continuity

$$\frac{\partial r\rho u}{\partial x} + \frac{\partial r\rho v}{\partial r} = 0 \tag{7}$$

Species Diffusion for the i^{th} Specie:

$$\rho u \frac{\partial \alpha_i}{\partial x} + \rho v \frac{\partial \alpha_i}{\partial r} = \frac{1}{r} \frac{\partial}{\partial r} \left\{ r\rho \frac{\nu_T}{Sc} \left[\frac{\partial \alpha_i}{\partial r} \right] \right\} + \dot{w}_i \tag{8}$$

Momentum Equation:

$$\rho u \frac{\partial u}{\partial x} + \rho v \frac{\partial u}{\partial r} = \frac{1}{r} \left\{ \frac{\partial}{\partial r} \left(r\rho\nu_T \frac{\partial u}{\partial r} \right) \right\} - \frac{\partial p}{\partial x} \tag{9}$$

and the Energy Equation

$$\rho u \frac{\partial H}{\partial x} + \rho v \frac{\partial H}{\partial r} =$$

$$\frac{1}{r} \frac{\partial}{\partial r} \left\{ \frac{r\rho\nu_T}{Pr} \left[\frac{\partial H}{\partial r} - \left(\frac{Pr}{Sc} - 1 \right) \sum_i h_i \frac{\partial \alpha_i}{\partial r} + (Pr - 1) \frac{\partial}{\partial r} \left(\frac{u^2}{2} \right) \right] \right\} \tag{10}$$

in which Pr and Sc represent the Prandtl and Schmidt numbers, respectively. These equations, along with expressions for the enthalpy

$$H = h + \frac{u^2}{2} \text{ and } h = \sum_i \alpha_i h_i (T) \tag{11}$$

and the equation of state

$$p = \rho RT \sum_i (\alpha_i / W_i) \tag{12}$$

can be solved, given an expression for the turbulent momentum diffusivity ν_T, or the turbulent eddy viscosity $\mu_T = \rho\nu_T$. The problem of the most

appropriate formulation for the eddy viscosity in a turbulent flow has occupied the attention of researchers in turbulent flow for many years, and numerous proposals for the appropriate form of the eddy viscosity have been made. In general, up until a few years ago, models for the turbulent eddy viscosity involved a relation between a local length scale and a local measure of the velocity gradient. The free turbulent mixing model proposed by Prandtl in 1942 [10] is a case in point; with this model

$$\mu_T = \rho c b |\Delta u| \tag{13}$$

where c is a constant, b is a measure of the width of the mixing region, and Δu a measure of the velocity difference across the mixing region.

While eddy viscosity models have in certain circumstances enabled successful calculations of particular turbulent flows to be carried out, in general, the constant of proportionality involved in the model varies markedly and unpredictably in different flowfields [11].

The observed lack of generality of eddy viscosity models has led to the development of a class of models in which additional partial differential equations are written to obtain the spatial variation of the shear stress. Of these, one of the most highly developed is the two-equation turbulent kinetic energy model developed by Launder, et al. [7], in which transport equations are written for the turbulent kinetic energy

$$k = \frac{1}{2}\left(\overline{u'^2 + v'^2 + w'^2}\right) \tag{14}$$

and its dissipation rate, ε. In boundary layer form, these equations can be written:

Turbulent Kinetic Energy

$$\rho u \frac{\partial k}{\partial x} + \rho v \frac{\partial k}{\partial r} = \frac{1}{r}\frac{\partial}{\partial r}\left(\frac{\mu_T r}{\sigma_k}\frac{\partial k}{\partial r}\right) + \mu_T\left(\frac{\partial u}{\partial r}\right)^2 - \rho\varepsilon \tag{15}$$

Turbulence Energy Dissipation

$$\rho u \frac{\partial \varepsilon}{\partial x} + \rho v \frac{\partial \varepsilon}{\partial r} = \frac{1}{r} \frac{\partial}{\partial r}\left(\frac{\mu_T r}{\sigma_\varepsilon} \frac{\partial \varepsilon}{\partial r}\right) + C_{E1} \frac{\varepsilon}{k} \mu_T \left(\frac{\partial u}{\partial r}\right)^2 - C_{E2} \rho \frac{\varepsilon^2}{k} \tag{16}$$

where

$$\mu_T = C_\mu \rho k^2/\varepsilon \tag{17}$$

and in which

$$C_\mu = 0.09,\ C_{E1} = 1.40,\ C_{E2} = 1.95 \tag{18}$$

The turbulence energy dissipation rate, ε, can be related to a turbulent length scale, ℓ_k, through the Kolmogorov hypothesis

$$\varepsilon \propto k^{3/2}/\ell_k \tag{19}$$

so that the transport equation for turbulence energy dissipation can also be regarded as a description of the spatial variation of the turbulent length scale.

2.3 CHEMICAL KINETICS: THE QUASIGLOBAL MODEL

In both the stirred reactor and directed flow portions of the modular model volumetric chemical kinetic production rate terms appear in the species transport equations. These terms can be evaluated using a full hydrocarbon chemical kinetics scheme based on the quasiglobal kinetics model [6], which has as a key element a subglobal oxidation step

$$C_nH_m + \frac{n}{2} O_2 \rightarrow \frac{m}{2} H_2 + nCO \tag{20}$$

This reaction is unidirectional with an empirically determined rate (grams of fuel/cc/sec) given by

$$A T^b P^{0.3} \left[C_n H_m\right]^{\frac{1}{2}} \left[O_2\right] \exp\left[-E/RT\right] \qquad (21)$$

with the constants A, b, and E/R defined in Table 2, where P must be given in atmospheres, T in degrees Kelvin and [ ] denotes molar concentration; coupled to this subglobal step are the intermediate reversible reactions given in Table 2.

Table 2. EXTENDED C-H-O CHEMICAL KINETIC REACTION MECHANISM

$$k_f = AT^b \exp(-E/RT)$$

Reaction	A	Forward	E/R
1) $C_nH_m + \frac{n}{2}O_2 \rightarrow \frac{m}{2}H_2 + n\,CO$ *	A. Long Chain 6.0×10^4	1	12.2×10^3
	B. Cyclic 2.08×10^7	1	19.65×10^3
2) $CO + OH = H + CO_2$	5.6×10^{11}	0	0.543×10^3
3) $CO + O_2 = CO_2 + O$	3.0×10^{12}	0	25.0×10^3
4) $CO + O + M = CO_2 + M$	1.8×10^{19}	-1	2.0×10^3
5) $H_2 + O_2 = OH + OH$	1.7×10^{13}	0	24.7×10^3
6) $OH + H_2 = H_2O + H$	2.19×10^{13}	0	2.59×10^3
7) $OH + OH = O + H_2O$	5.75×10^{12}	0	0.393×10^3
8) $O + H_2 = H + OH$	1.74×10^{13}	0	4.75×10^3
9) $H + O_2 = O + OH$	2.24×10^{14}	0	8.45×10^3
10) $H + O + H = OH + H$	1.0×10^{16}	0	0
11) $H + O + O = O_2 + H$	9.38×10^{14}	0	0
12) $H + H + H = H_2 + H$	5.0×10^{15}	0	0
13) $H + H + OH = H_2O + H$	1.0×10^{17}	0	0
14) $O + N_2 = N + NO$	1.36×10^{14}	0	3.775×10^4
15) $N_2 + O_2 = N + NO_2$	2.7×10^{14}	-1.0	6.06×10^4
16) $N_2 + O_2 = NO + NO$	9.1×10^{24}	-2.5	6.46×10^4
17) $NO + NO = N + NO_2$	1.0×10^{10}	0	4.43×10^4
18) $NO + O = O_2 + N$	1.55×10^9	1.0	1.945×10^4
19) $M + NO = O + N + M$	2.27×10^{17}	-0.5	7.49×10^4
20) $M + NO_2 = O + NO + M$	1.1×10^{16}	0	3.30×10^4
21) $M + NO_2 = O_2 + N + M$	6.0×10^{14}	-1.5	5.26×10^4
22) $NO + O_2 = NO_2 + O$	1.0×10^{12}	0	2.29×10^4
23) $N + OH = NO + H$	4.0×10^{13}	0	0
24) $H + NO_2 = NO + OH$	3.0×10^{13}	0	0
25) $CO_2 + N = CO + NO$	2.0×10^{11}	-1/2	4.0×10^3
26) $CO + NO_2 = CO_2 + NO$	2.0×10^{11}	-1/2	2.5×10^3

* $$\frac{d[C]_{C_nH_m}}{dt} = -A T^b P^{0.3} C_{C_nH_m}^{1/2} C_{O_2} \exp\left(-\frac{E}{RT}\right);$$

$$[C] = \frac{gm\ moles}{cc},\ [T] = {}^oK,\ [P] = atm.,\ [E] = \frac{kcal}{mole}$$

Reverse reaction rate k_r is obtained from k_f and the equilibrium constant K_c

2.4 MODELS FOR THE FUEL INJECTION PROCESS

In addition to the basic components of a parabolic, directed flow analysis and a well-stirred reactor formulation, the modular concept can be extended to include modules which represent other elements of the dump combustor flowfield, for example, the fuel injection process. The detail of the computation provided by the use of a parabolic directed flow analysis (as opposed to the relative coarseness of the numerical grid allowable in current unified, elliptic solution techniques) is the key feature of the modular model that allows the inclusion of a fuel injection module in the complete analysis. This is particularly true in the case of liquid fuel injection, for at the fuel/air ratios appropriate for dump combustor operation, the liquid fuel streams initially occupy a very small portion of the overall combustor cross-sectional area. It is also worth noting that it has been stated that the further development of unified, elliptic combustor flowfield calculations requires the development of what are essentially modular models for such features as the fuel injection process [2] since these key processes occur on scales much smaller than feasible numerical resolution allows. Thus the development of fuel injection, vaporization, and spreading models through use of the overall modular model concept is necessary for further development of unified techniques.

The liquid fuel injection model makes use of a combination of empirical information and turbulent mixing calculations. For example, the fuel jet penetration from the wall is computed through the use of the penetration correlation developed by Catton, Hill and McRae [12], using the breakup time correlation developed by Clark [13] to compute the downstream distance at which penetration is to be computed. That is, it is assumed that the fuel jet has turned parallel to the airflow at the axial position at which the initial fuel jet has broken up into droplets, as given by the breakup time correlation and the local airflow velocity.

Since the basic modular model formulation involves an axisymmetric flowfield, individual fuel jets cannot be resolved, and it is assumed in the formulation that the liquid fuel spray forms an annulus

whose cross-sectional area may either be specified or computed based on an assumed fuel spray bulk velocity. A bulk spray evaporation correlation is then used to compute the fuel vaporization rate; this correlation, developed by Ingebo and Foster [14] is a function of the initial velocity and temperature difference between the fuel spray and the surrounding air stream. Spreading of the fuel jet is computed through use of a turbulent mixing hypothesis as for the mixing process in the remainder of the parabolic flow.

Figure 2 shows the results of a computation of the fuel injection process for three fuel injectors, located in the combustor inlet wall, along the centerline, and in a midstream position. Shown are the computed contours of the fuel mass fraction, α_F, with the vapor-phase fuel shown as the solid line and the liquid phase fuel as the dotted line, as a function of both axial and radial position in the combustor inlet. For these calculations the air inlet velocity was approximately 700 ft/sec at a temperature of 1600^{o}K; the overall fuel-air equivalence ratio was 0.6. The results shown in Figure 2 provide a good example of the detail of the fuel injection process available through use of this aspect of modular modeling.

2.5 COUPLING RELATIONS AND ITERATION PROCEDURE

The overall logic of the calculation procedure is shown schematically in Figure 3. Inlet conditions can be defined upstream or downstream of the fuel injection station as required; if liquid fuel injection is specified, the penetration and spreading of the liquid fuel jets are computed as described in the preceding section. The computation proceeds to the dump plane in the sudden expansion combustor, at which point the dependent variables in the flowfield are stored for later use in the recirculation zone iteration procedure.

An initial state for the stirred reactor must be specified in order to begin the iteration procedure. This state is reasonably arbitrary, except that a reacted temperature level must be specified. The shape of the dividing streamline separating the directed flow and the

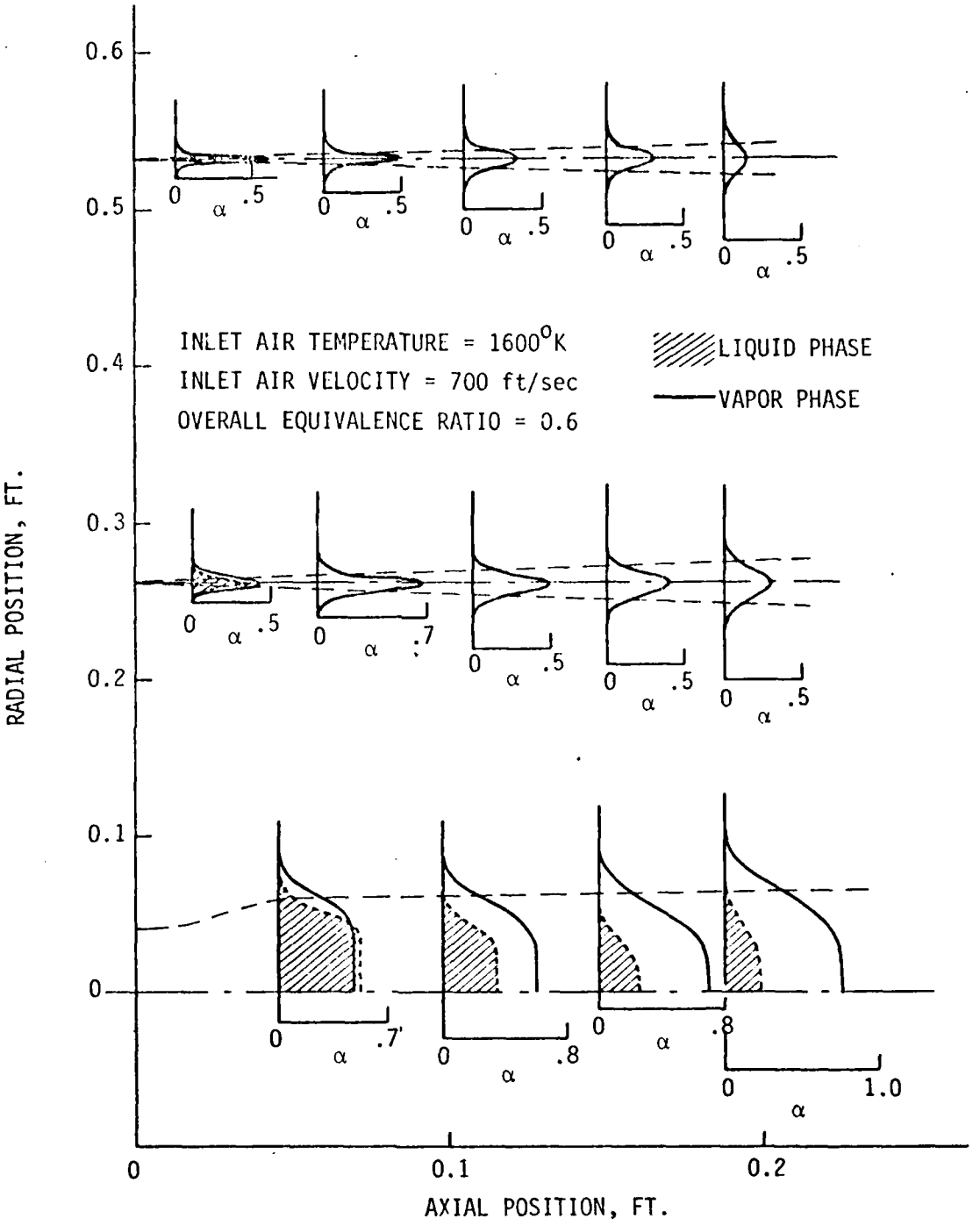

Figure 2. PREDICTED FUEL MASS FRACTION DISTRIBUTIONS FOR SIMULTANEOUS INJECTION AT THREE RADIAL LOCATIONS

recirculation zone must also be specified, along with the shear stress level, expressed as a "skin friction" coefficient. The initial stirred reactor state, in conjunction with a model for the shear layer existing in the combustor flowfield between the recirculation zone and the directed flow then defines the boundary conditions for the parabolic directed flow calculation. Directed flow computations are carried out to the axial station at which the end of the recirculation zone has been defined; as part of these computations the diffusive flux of species and energy across the dividing streamline is computed. These fluxes then define a new set of stirred reactor "feed rates", i.e., species and energy fluxes into the recirculation zone region.

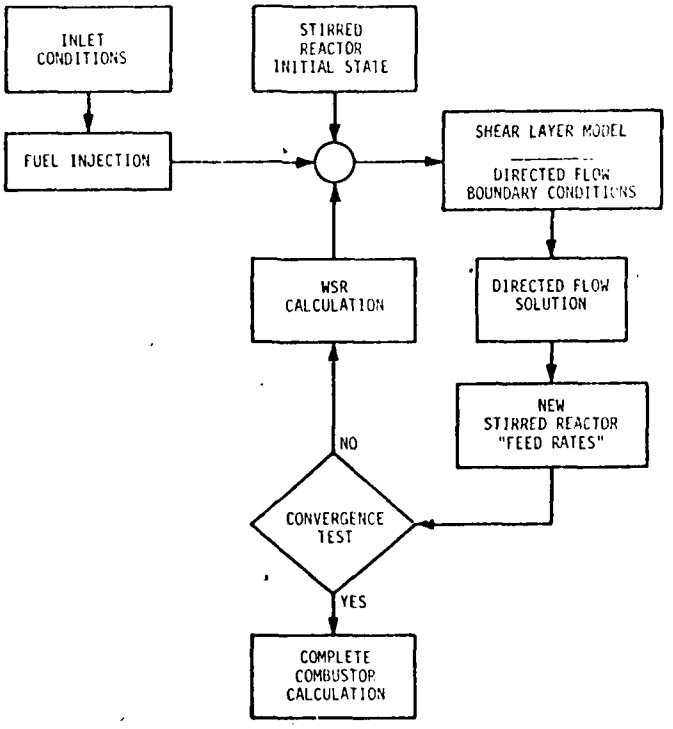

Figure 3. MODULAR MODEL CALCULATION LOGIC

Convergence of the procedure is defined by the change in the stirred reactor feed rates from iteration to iteration; each species and the energy flux must change less than 0.1% before the convergence criteria are satisfied. If they are not, the species and energy fluxes, and the overall diffusive mass flux and physical recirculation zone volume are used to compute a new stirred reactor state. The pressure required for this computation is taken to be the arithmetic average of the pressures computed as part of the directed flow solution at the beginning and end of recirculation region. The new stirred reactor state is then used to define new directed flow boundary conditions, and the computation is restarted from the dump station. When convergence is achieved, typically in 3-5 iterations, the combustor calculation is continued to the specified combustor exit station.

As will be noted in the description which follows, there are a number of specifiable constants in this flowfield model, including the length of the recirculation zone, the recirculation zone shape, the initial thickness and spread rate of the shear layer along the dividing streamline, and the dividing streamline shear stress distribution. Both the size and shape of the recirculation zone can be adequately specified as functions of the dump combustor geometry, and it has been found that the shear layer initial thickness, spread rate, and shear stress distribution along the dividing streamline have a marked effect on the static pressure distribution computed for the combustor. This suggests that an outer iteration loop can be used to adjust the computation for a specific combustor geometry through matching of the computed static pressure profile with experimental data for that geometry, and as will be described in Section 3, this technique has been successfully used to match computed and experimental distributions of static pressure for both cold flow and reacting flow, through adjustment of the specifiable constants in the model.

In describing the coupling between the stirred reactor and directed flow elements of the module, it is useful, for clarity, to consider a simplified formulation for the stirred reactor, using a global finite rate kinetics model. In this model, the fuel consumption rate is given by the expression

$$\frac{dC_F}{dt} = -C_F C_{O2}^{3/2} A \exp(-B/RT) \tag{22}$$

where the C's have the units (moles/cc/sec), T is in ^{O}K, and R is in kcal/mole ^{O}K; $A = 3.80 \times 10^{15}$ and $B = 15{,}600$. Performing the manipulations necessary to recast Eq. 22 in terms of mass fractions, and substituting into Eq. 2, results in a set of simultaneous equations for the active species of the form:

$$\frac{dM\alpha_{O_2}}{dt} = \dot{m}^I_{O_2} - W_{O_2}\alpha_F \alpha_{O_2}^{3/2} V \theta(T) \tag{23}$$

$$\frac{dM\alpha_F}{dt} = \dot{m}^I_p - W_F \frac{\alpha_F \alpha_{O_2}^{3/2}}{(n + m/4)} V \theta(T) \tag{24}$$

$$\frac{dM\alpha_{CO_2}}{dt} = \dot{m}^I_{CO_2} - W_{CO_2}\left(\frac{n}{n + m/4}\right)\alpha_F \alpha_{O_2}^{3/2} V \theta(T) \tag{25}$$

$$\frac{dM\alpha_{H_2O}}{dt} = \dot{m}^I_{H_2O} + W_{H_2O}\left(\frac{m/2}{n + m/4}\right)\alpha_F \alpha_{O_2}^{3/2} V \theta(T) \tag{26}$$

$$\frac{dM\alpha_{N_2}}{dt} = \dot{m}^I_{N_2} \tag{27}$$

where n and m are the carbon and hydrogen atoms in the general fuel molecule C_nH_m, the W's are the molecular weights of the species, and

$$\theta(T) = \rho^{3/2} A \exp(-B/RT)/W_F W_{O_2}^{3/2} \tag{28}$$

Given the specification of the $\dot{m}^I_i$, Eq. 23-27, along with the perfect gas

equation of state and Eq. 3 are solved to obtain the new steady-state values of the active species, i.e., the values obtained when

$$\frac{dM\,\alpha_i}{dt} \to 0$$

A key element in the modular formulation is the model for the shear layer between the recirculation zone and the directed flow. It is the computation in this region that provides the boundary conditions for the parabolic directed flow calculation; through the gradients in energy and species mass fractions computed from the directed flow solution, the influx rates $\dot{m}_i^I$ in Eq. 23-27 and the energy flux h^I in Eq. 3 are evaluated.

In the modular model the shear layer region is computed in a simplified form: it is assumed that the shear layer can be modeled as a region $\ell(x)$ across which all dependent variables (i.e., velocity, temperature, species mass fractions) vary linearly. It is further assumed that the shear layer width itself is specifiable by a linear growth law,

$$\ell = ax + b \tag{29}$$

in which a and b are constants. The constant b can be related to the initial boundary layer thickness at the expansion plane, while a can be related to empirical expressions for shear layer growth rate. It might further be noted that for self-similar shear layers, the constant a can be related to the shear stress level at some characteristic point in the shear layer. However, for reacting sudden-expansion burner flows self-similar shear layer concepts do not apply and the dividing streamline shear stress is, in the modular model, independently specifiable.

As shown in Figure 4, the dividing streamline shape $R_c(x)$ is specified: this specification also defines the dividing streamline stream function value ψ_w. Along $\psi = \psi_w$, the turbulent shear stress is specified through the use of an input "skin friction coefficient":

$$C_{FW} = \tau_w / \tfrac{1}{2} \bar{\rho}\, \bar{U}^2 \tag{30}$$

where $\bar{\rho}$ and $\bar{U}$ are evaluated as the average of their values along the flowfield centerline and along the streamline $\psi = \psi_p$. As noted above, temperature and species mass fractions are assumed to vary linearly across the shear layer. If ψ_p is defined as the streamline immediately "outside" the recirculation region (i.e., within the directed flow) and ψ_r is a (an imaginary) streamline immediately "inside" the recirculation zone, then, for species i

$$\left.\frac{\partial \alpha_i}{\partial r}\right)_w = \frac{\alpha_{ip} - \alpha_{ir}}{\ell(x)} \tag{31}$$

and for temperature

$$\left.\frac{\partial T}{\partial r}\right)_w = \frac{T_p - T_r}{\ell(x)} \tag{32}$$

where α_{ir} and T_r are the values of the species mass fractions and temperature obtained from the stirred reactor solution.

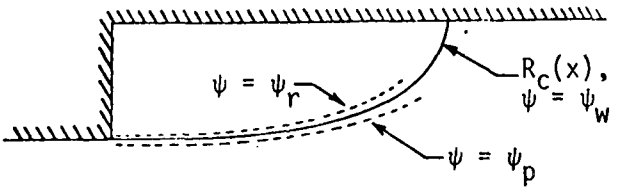

Figure 4. DIVIDING STREAMLINE DEFINITION SKETCH

The boundary conditions at $\psi = \psi_w$ established by Eq. 30-32 define, through the parabolic solution, effective gradients which, through turbulent diffusion, can be used to define the influx into the stirred reactor. For example, we can write

$$\dot{m}_i^I = 2\pi \int_0^L -\rho \frac{\nu_T}{Sc} \frac{\partial \alpha_i}{\partial r} R_c(x)\, dx \tag{33}$$

where L is the distance measured along the dividing streamline and ν_T the turbulent diffusivity for momentum; Sc is the Schmidt number. In discretized form (Appendix I), using the transformation

$$\rho u r dr = \psi\, d\psi \tag{34}$$

Eq. 33 can be rewritten

$$\dot{m}_i^I = \frac{-\pi}{Sc} \int_0^L \frac{d}{\Delta\psi} (\alpha_i^r - \alpha_i^p) R_c(x)\, dx \tag{35}$$

where $d \equiv \rho u r^2 \mu_T/\psi$ and $\mu_T = \rho\nu_T$. Defining

$$\bar{\alpha}_i^p = \int_0^L \frac{d}{\Delta\psi} \alpha_i^p R_c(x)\, dx \Big/ \int_0^L \frac{d}{\Delta\psi} R_c(x)\, dx \tag{36}$$

and noting that, by definition, α_i^r is constant,

$$\dot{m}_i^I = \frac{-\pi}{Sc} \int_0^L \frac{d}{\Delta\psi} R_c(x)\, dx \left\{\alpha_i^r - \bar{\alpha}_i^p\right\} = -\dot{m}_D^I (\alpha_i^r - \bar{\alpha}_i^p) \tag{37}$$

Substituting Eq. 37 into Eq. 2, and taking $dM\alpha_i/dt = 0$ results in the working form of the well-stirred reactor species equation used in the modular model,

$$\alpha_i^r\Big|_{n+1} = \bar{\alpha}_i^p\Big|_n + \dot{w}_i V/\dot{m}_a^I \tag{38}$$

where n and n + 1 are sequential elements of the iteration loop shown in Figure 3.

A similar development can be followed for the energy flux term h^I in Eq. 3. For unity Lewis number, the result is

$$h^r\Big|_{n+1} = \left(\bar{h}^p\Big|_n + \frac{\dot{Q}}{\dot{m}_d^I}\right)\Bigg/\left[1 + \sum_i (\bar{\alpha}_i^p - \alpha_i^r)\Big|_n\right] \tag{39}$$

where the summation is taken only over influx species, i.e., species for which $\alpha_i^r < \bar{\alpha}_i^p$.

With the describing equations derived, the iteration procedure involved in the modular model can be restated. Given the conditions in the directed flow at the start of the recirculation zone, either by calculation of the process occuring upstream of the dump station or as input conditions, and given initial guesses for the recirculation zone state, α_i^r and T^r, as well as the geometric variables $R_c(x)$ and a and b in the shear layer width expression, Eq. 29, and the "skin friction coefficient" C_{FW}, the parabolic calculation proceeds to the end of the recirculation zone, using Eq. 30-32 as boundary conditions. When the end of the recirculation zone is reached, $\bar{\alpha}_i^p$, $\bar{h}^p$, and $\dot{m}_D^I$ are evaluated, and these quantities are used, along with an input specification of $\dot{Q}$, to compute a new stirred reactor state from Eq. 23-28. The process is repeated until changes smaller than 0.10% are observed in $\bar{\alpha}_i^p$ and $\bar{h}^p$, after which the remainder of the combustor calculation is carried out.

Boundary conditions for the turbulent kinetic energy, k, and the turbulent kinetic energy dissipation rate, ε, are established in the same manner as described for the mean total energy and species equations. Thus, values are assumed for the turbulent kinetic energy and dissipation length scale for the stirred reactor region, k_r and ε_R, respectively, and the gradient in k and ε along the dividing streamline established from the relations

$$\frac{\partial k}{\partial r}\Big)_w = \frac{k_p - k_r}{\ell(x)} \tag{40}$$

and

$$\left.\frac{\partial \varepsilon}{\partial r}\right)_w = \frac{\varepsilon_p - \varepsilon_r}{\ell(x)} \tag{41}$$

As is evident from this discussion, a number of parameters must be specified, either empirically or through comparison of model predictions with experiment, for a modular model computation to proceed. These include the size and shape of the recirculation zone, the coefficients a and b in Eq. 29, the recirculation zone values of k and ε, and the dividing streamline skin friction coefficient C_{FW}. While this is a fairly lengthy list of coefficients, and is in addition to the inlet and wall boundary conditions that must be specified in any formulation, experience has shown that good results can be achieved using a reasonably limited range of values of these coefficients. However, it should be stressed that the modular approach is not a *predictive* tool in the sense that it can be relied upon in the absence of experimental data; instead, the model is one which, given a limited amount of available data, can be used to interpret the phenomena occuring within the combustor under test, and to provide a means for scaling limited test results to cover a more general range of interest to the combustor designer.

SECTION 3
APPLICATION OF MODULAR MODELING TO SUDDEN-EXPANSION FLOWFIELDS

In order to demonstrate the application of the modular model to the analysis and interpretation of sudden-expansion flowfield data, calculations of a variety of different sudden-expansion flows have been carried out. These flowfields include incompressible and compressible nonreacting flows and premixed reacting flows; in the latter case, both one-step global and the full quasiglobal chemical kinetics models have been used. Although there are a number of empirical coefficients in the model, these computations illustrate that coefficient values can be selected based on one set of data and, in large part, used for the computation of different flowfields: where changes in coefficients are required the differences in each case can be related to physical differences in the flowfields in different configurations.

3.1 COLD FLOW APPLICATIONS

Validation and demonstration of the modular model requires detailed data for the sudden-expansion configuration of interest. One such source of detailed data is the work reported by Chaturvedi [15] for an essentially incompressible sudden-expansion flowfield.

The sudden-expansion configuration investigated by Chaturvedi involved an area ratio of 4.0 with an inlet Reynolds number (based on inlet diameter) of 2×10^5. The inlet velocity was thus of the order of 100 ft/sec. A variety of expansion angles were studied, varying from 15^0 to 90^0; the 90^0 expansion angle case is of the most interest in this model validation work. Chaturvedi's apparatus had an L/D of 25 based on the inlet diameter and was aspirated by a centrifugal pump and butterfly valve assembly at the downstream end; the inlet was a bellmouth intake directly coupled to the expansion section. Because of the differences in Chaturvedi's experimental apparatus relative to a typical sudden-expansion

combustor configuration, which include the lack of an exhaust nozzle section, the greater mixing chamber length relative to a typical combustion chamber, and the lack of an inlet section, the modeling assumptions necessary to match the modular model predictions with these data are not necessarily appropriate for a sudden-expansion combustor. Nevertheless, Chaturvedi's data, which include axial and radial profiles of mean velocity, axial and radial turbulent intensity components, and total pressure, are detailed enough to provide a critical test of modeling capability.

The data used for the comparisons shown here have been obtained from that presented in Chaturvedi's paper [15]. Further, both the turbulent kinetic energy and wall static pressure data have been obtained by calculation from the data presented by Chaturvedi, and are thus based on assumptions not inherent in Chaturvedi's work. The turbulent kinetic energy has been obtained from Chaturvedi's u'/U_0 and v'/U_0 data using the assumption $w'/U_0 = \frac{1}{2}\, v'/U_0$, while the wall static pressure has been derived from measured centerline total pressure and velocity data using Bernoulli's equation and the assumption that the static pressure is radially constant.

The parameters, in addition to wall boundary conditions and inlet conditions, that must be specified for a modular computation include:

- recirculation zone size and shape
- shear layer initial thickness and growth rate
- dividing streamline shear stress coefficient
- recirculation zone turbulent kinetic energy level
- recirculation zone turbulent dissipation length scale

Previous work had established that the dividing streamline shape was well represented by a parabolic arc arranged such that at the step, $dr/dx = 0$, and which intercepts the wall at a distance 9.2 step heights from the inlet. The recirculation zone length correlation used here was based on Drewry's results [16]. Previous work also showed that the dividing streamline shear stress coefficient had a strong effect on the predicted static pressure distribution, while the turbulent kinetic energy dissipation rate

length scale assumed for the recirculation zone had a strong effect on the rate of transport into and out of the recirculation region. The shear layer initial thickness and rate of growth had little overall effect, over the range considered in the earlier work.

Although Chaturvedi's data show a reattachment point at 9.2 step heights from the inlet and indicate an essentially parabolic recirculation zone shape, comparison of the predictions of the model with the data for static pressure and centerline velocity showed that these data could not be reproduced with the parabolic recirculation zone boundary that has been used in other modular model calculations. Instead, an extended recirculation zone shape had to be adopted. Figure 5 illustrates the experimentally determined recirculation zone shape, and the parabolic and modified recirculation zone shapes adopted for the computation. Note that when the extended shape is used, the effective recirculation zone length for purposes of computing the stirred reactor volume is kept at the 1.61 ft. distance indicated by the data; thus the extension represents a crude model of a region over which the displacement effect of the shear layer bounding the dividing streamline relaxes to that of a wall boundary layer.

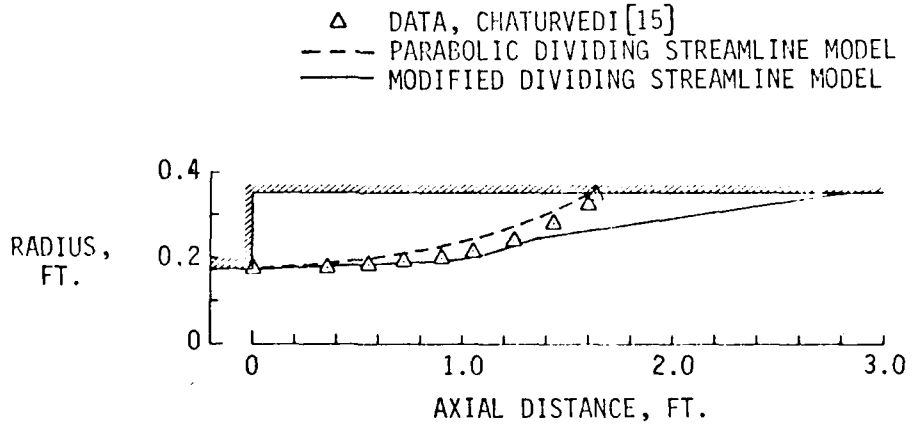

Figure 5. COMPARISON OF ASSUMED DIVIDING STREAMLINE SHAPES WITH CHATURVEDI DATA [15]

Centerline velocity and turbulent kinetic energy profiles and wall static pressure distributions are shown in Figure 6 in comparison with Chaturvedi's data [15]. For these calculations, the initial velocity was taken to be uniform across the inlet, at 100 ft/sec, the initial turbulent kinetic energy level was $10^{-4}U_0^2$, based on Chaturvedi's data, and the initial turbulence energy dissipation rate was obtained from $\varepsilon = 1.69k^{1.5}/\ell_k$ with $\ell_k = 0.1\ r_0$. A standard set of two-equation model coefficients have been used for all of the flowfield computations reported in this paper; thus:

$$C_\mu = 0.09;\ C_{E1} = 1.40;\ C_{E2} = 1.95;\ \sigma_k = 1.00;\ \sigma_\varepsilon = 1.22.$$

Results are shown for two values of the effective shear stress coefficient along the dividing streamline, with $C_{FW} = 0.016$ providing the best agreement with the data for wall static pressure and centerline velocity, but underpredicting the centerline kinetic energy data. Note that the initial increase of the centerline kinetic energy is not predicted by the turbulence model used here; this phenomenon, which is associated with the closure of the potential core region of the flow, has also been observed in free jets. The other model parameters used in this calculation are $a = 0.03$, $b = 0.09$, $k_{RZ} = 0.005\ U_0^2$, and $\ell_{RZ} = (h + L_{RZ})/2$, where the latter two variables represent the effective turbulent kinetic energy and dissipation length scale within the recirculation region. In the expression for the recirculation zone length scale, h is the step height and L_{RZ} the recirculation zone length; since $L_{RZ} = 9.2\ h$, effectively $\ell_{RZ} = 5.1\ h$.

The predicted velocity profiles are compared with the experimental data on Figures 7 and 8. Overall, the agreement is reasonably good, although it is clear that the flowfield mixing rate is slightly overpredicted. For X/D = 2 and X/D = 4, the predicted velocity profiles end at the dividing streamline location, since the modular model does not provide any detail of the recirculation region flowfield. Figure 9 shows a comparison of predicted radial turbulent kinetic energy profiles at axial locations downstream of the recirculation zone; again the overall level of agreement is reasonably good.

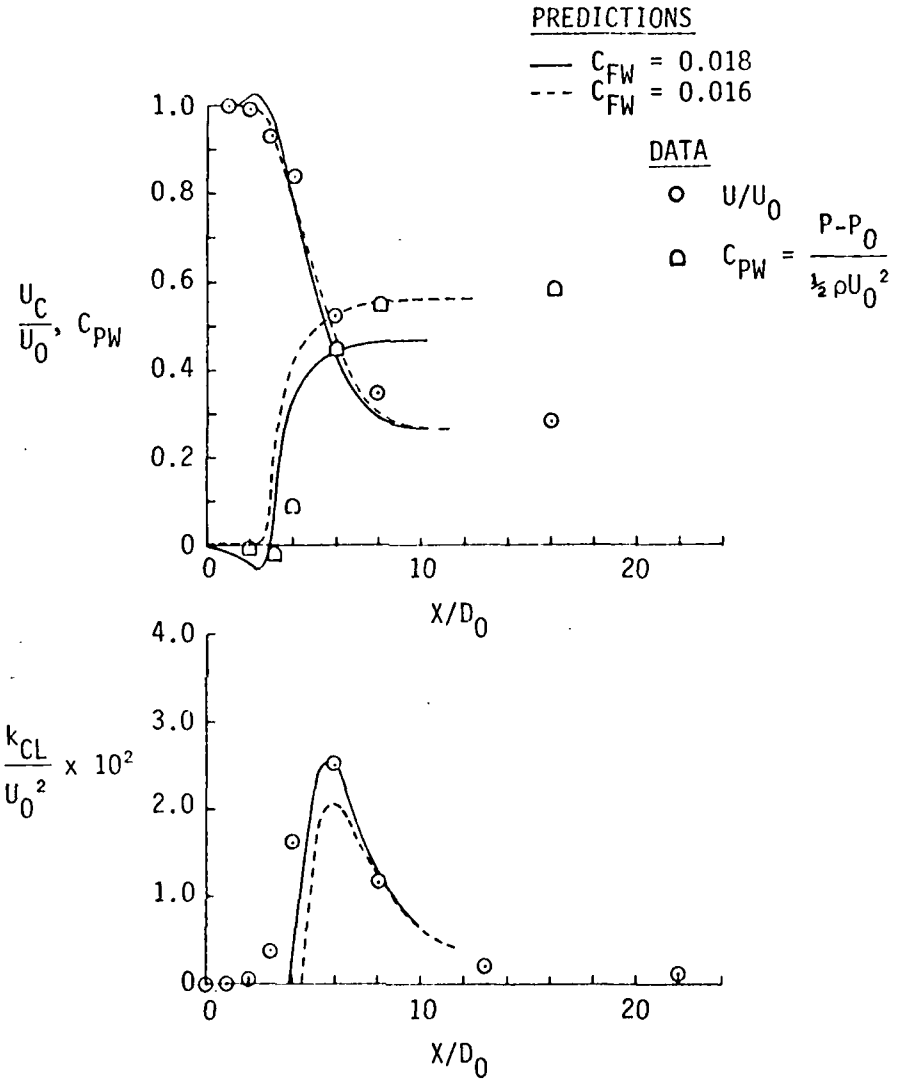

Figure 6. CENTERLINE VELOCITY AND TURBULENT KINETIC ENERGY PROFILES AND WALL PRESSURE COEFFICIENT, CHATURVEDI DATA [15]

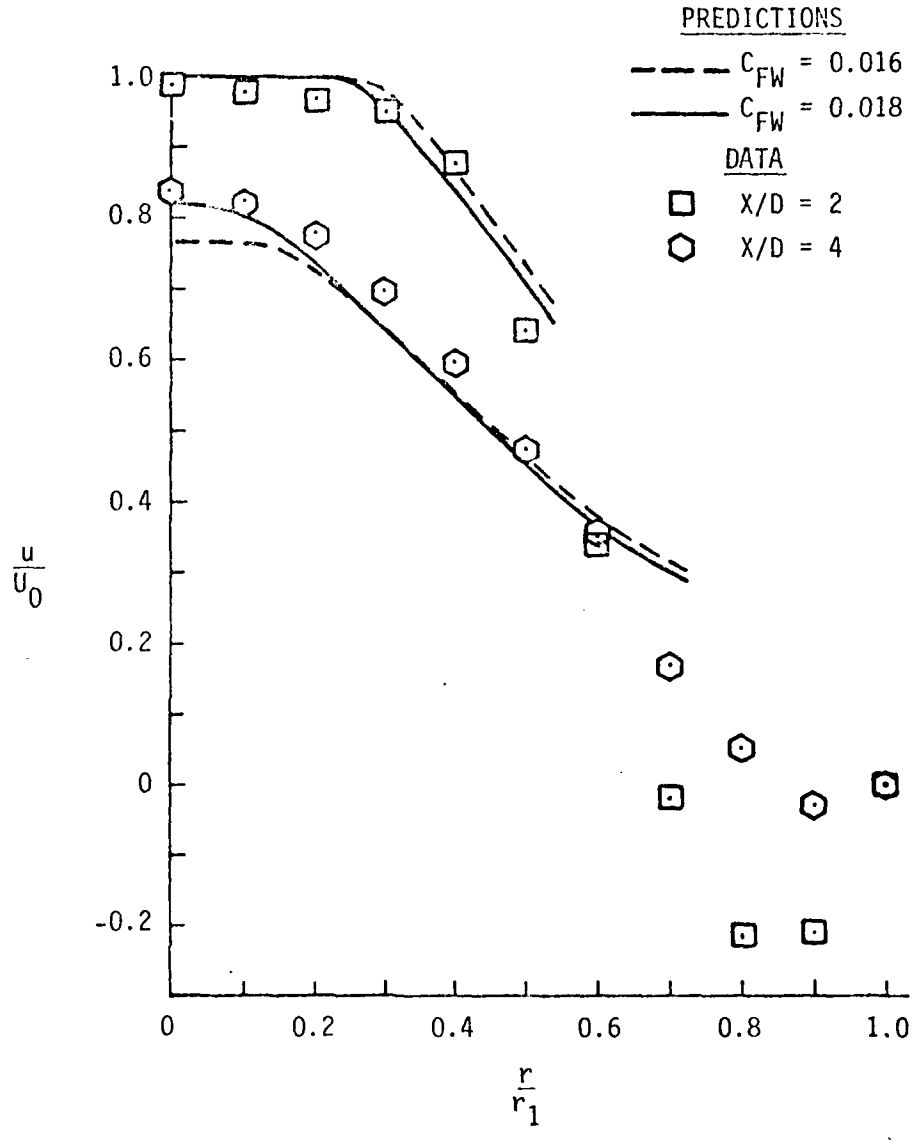

Figure 7. RADIAL VELOCITY PROFILES, CHATURVEDI DATA [15]

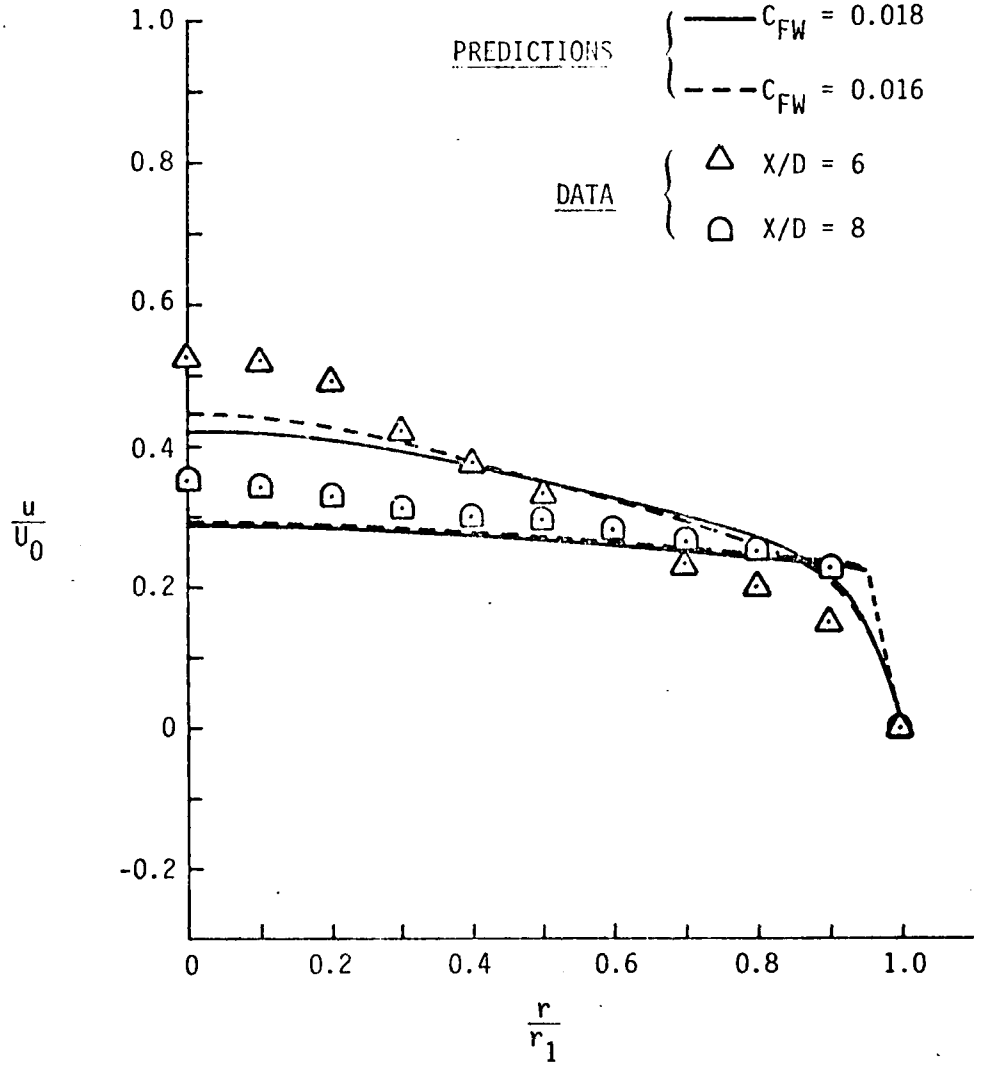

Figure 8. RADIAL VELOCITY PROFILES, CHATURVEDI DATA [15]

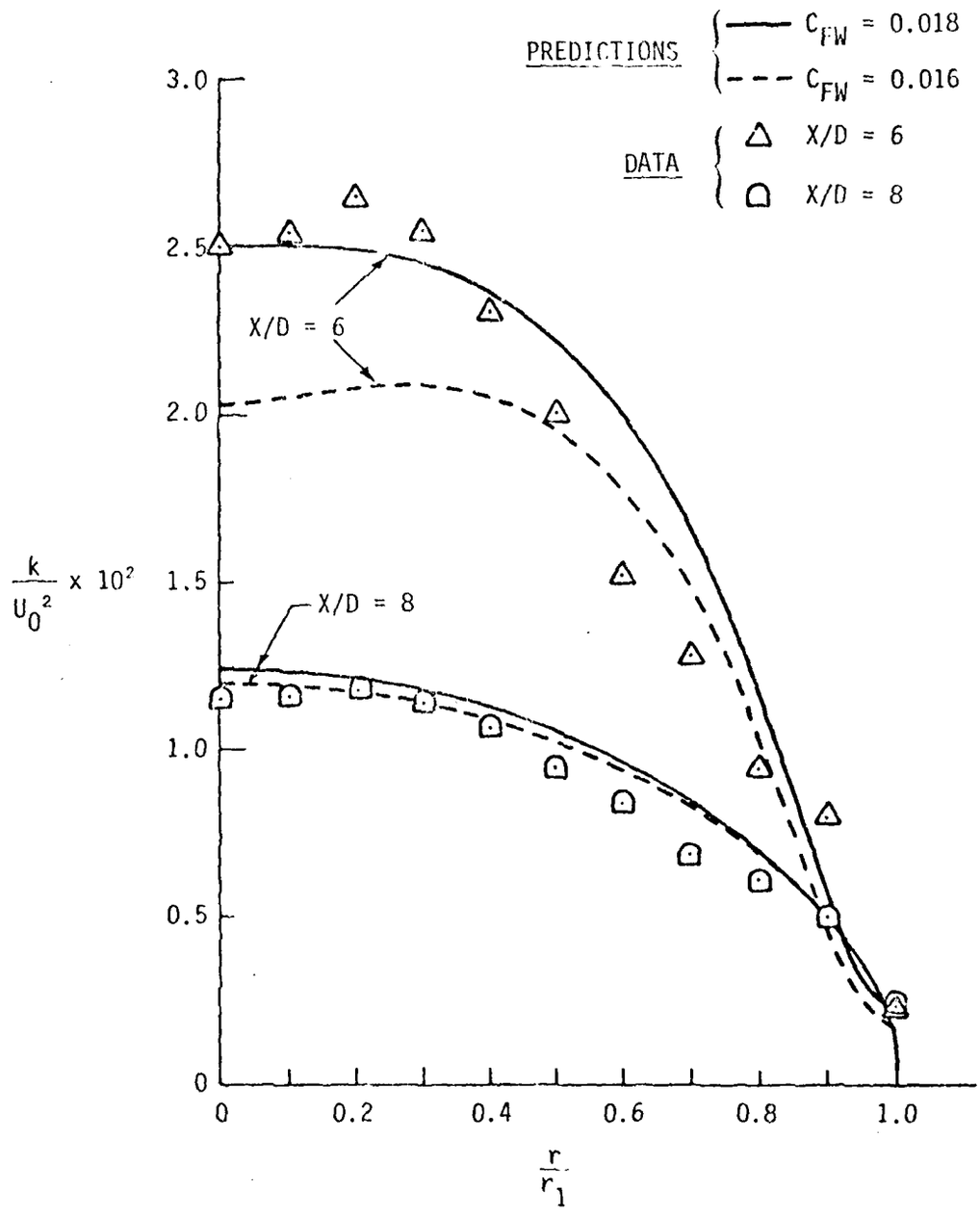

Figure 9. RADIAL TURBULENT KINETIC ENERGY PROFILES, CHATURVEDI DATA [15]

This comparison provides some validation of the ability of the modular approach to model accurately the details of a given flowfield. It is important to note that the adjustment of the model parameters carried out for this case was done with reference to the wall static pressure and centerline velocity measurements: the detailed profile data were not used in the modeling iteration. In the course of the modeling of this flowfield, a number of observations of model sensitivities were made:

- the predictions were insensitive to the parameters a and b in the shear layer growth model;
- the initial level of turbulent kinetic energy had a strong effect on the overall turbulent kinetic energy distribution in the flowfield, but a significantly smaller effect on the wall pressure distribution;
- the wall pressure distribution is primarily influenced by the size and shape of the recirculation zone and by the level of the assumed dividing streamline shear stress coefficient, C_{FW}.

It was noted earlier that the incompressible sudden-expansion represents a configuration for which the computational capabilities of the modular and unified models overlap, so that for this flowfield a comparison of results obtained using both types of model is of considerable interest. To provide this comparison, calculations of the Chaturvedi sudden expansion flowfield were carried out using an elliptic code developed from the Imperial College primitive variables formulation [17]. The inlet conditions and turbulence modeling used for the elliptic calculation were identical to that used in the modular approach; wall boundary conditions for the elliptic computations were defined using a "wall-function" technique [17] and the downstream boundary condition was obtained through use of a zero axial gradient hypothesis for all dependent variables. The unified model calculation used a 100 x 25 (x - r) grid to minimize numerical diffusion problems, and was continued for 1200 iterations to obtain a "mass imbalance" convergence criterion of less than 0.01%.

Comparisons of radial velocity profiles obtained through use of the unified model with those obtained from the modular calculation

and with Chaturvedi's [15] experimental data are shown in Figures 10 and 11. It is evident from these figures that the unified model predicts a greater mixing rate and shorter recirculation zone length than the data indicate; however, no effort was made to optimize the unified model calculations for these data (through, for example, modifications to the wall boundary conditions used in the computation). It is interesting to note that for X/D = 2 and X/D = 4, the unified model velocity profile shape predictions are similar to those the modular model produces, up to the dividing streamline. The modular model, of course, provides no detail within the recirculation region. Also of interest is the steepening of the velocity profile in the near wall region between X/D = 6 and X/D = 8 that is predicted by both models, Figure 11. This provides further evidence that the shear layer relaxation region hypothesized to exist in the modular model formulation of the flowfield is in fact a feature of this flow.

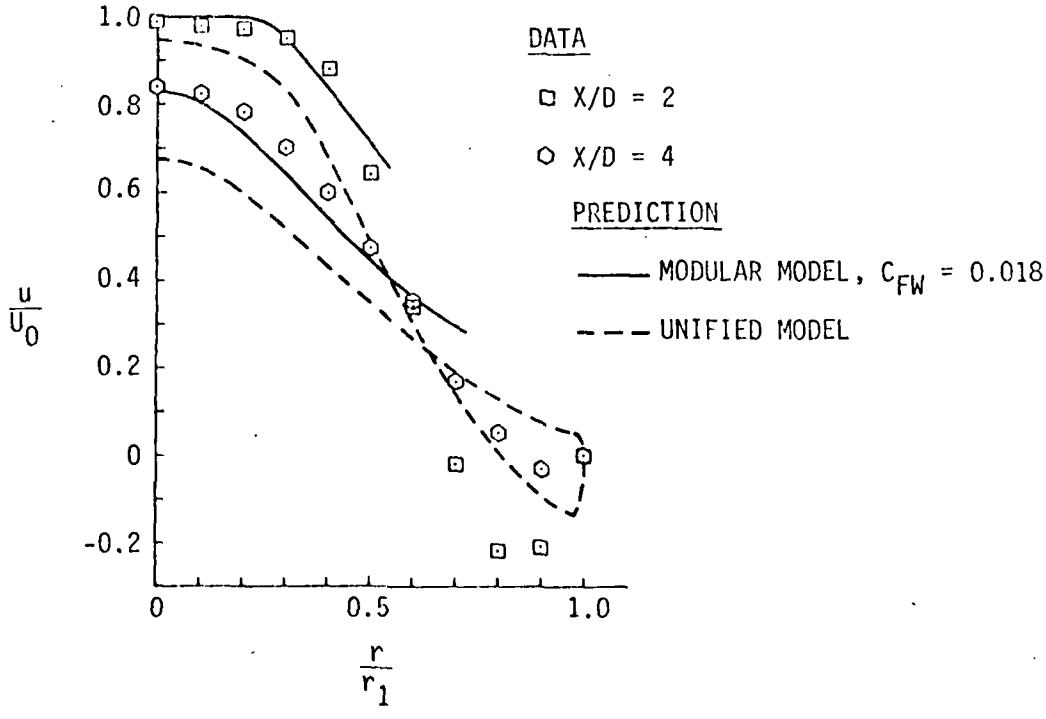

Figure 10. COMPARISON OF VELOCITY PROFILES PREDICTED BY MODULAR AND UNIFIED MODELS WITH DATA OF CHATURVEDI [15]

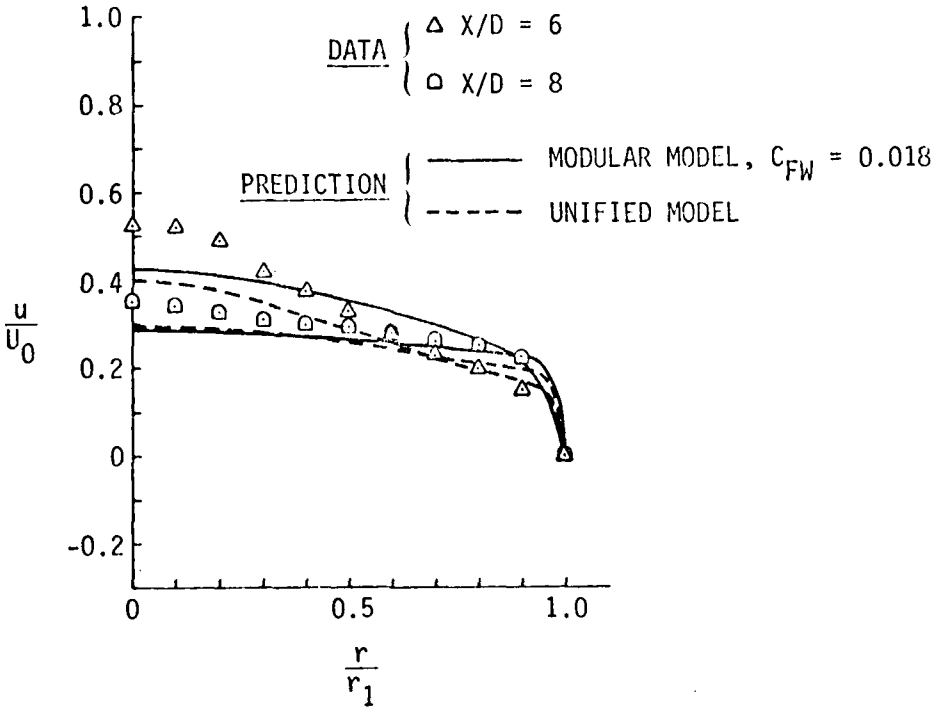

Figure 11. COMPARISON OF VELOCITY PROFILES PREDICTED BY MODULAR AND UNIFIED MODELS WITH DATA OF CHATURVEDI [15]

Radial turbulent kinetic energy profiles for X/D = 6 are shown in Figure 12. Although the elliptic model produces a slightly lower level of turbulent kinetic energy than does the modular approach, both calculations are in reasonably good agreement with the data.

These comparisons indicate that for this configuration, the modular approach is capable of providing predictions of the details of the flowfield that are in agreement with both the experimental data and with predictions obtained from unified techniques. Although, as has been noted previously, the modular model is not a *predictive* technique in the sense that unified approaches are intended to be, these comparisons indicate that the shear layer and recirculation zone modeling inherent in the modular approach are both adequate representations of these regions. This provides further validation of the modular model approach which, for

reacting sudden expansion flows, is capable of providing far more detail than is practically available with unified techniques.

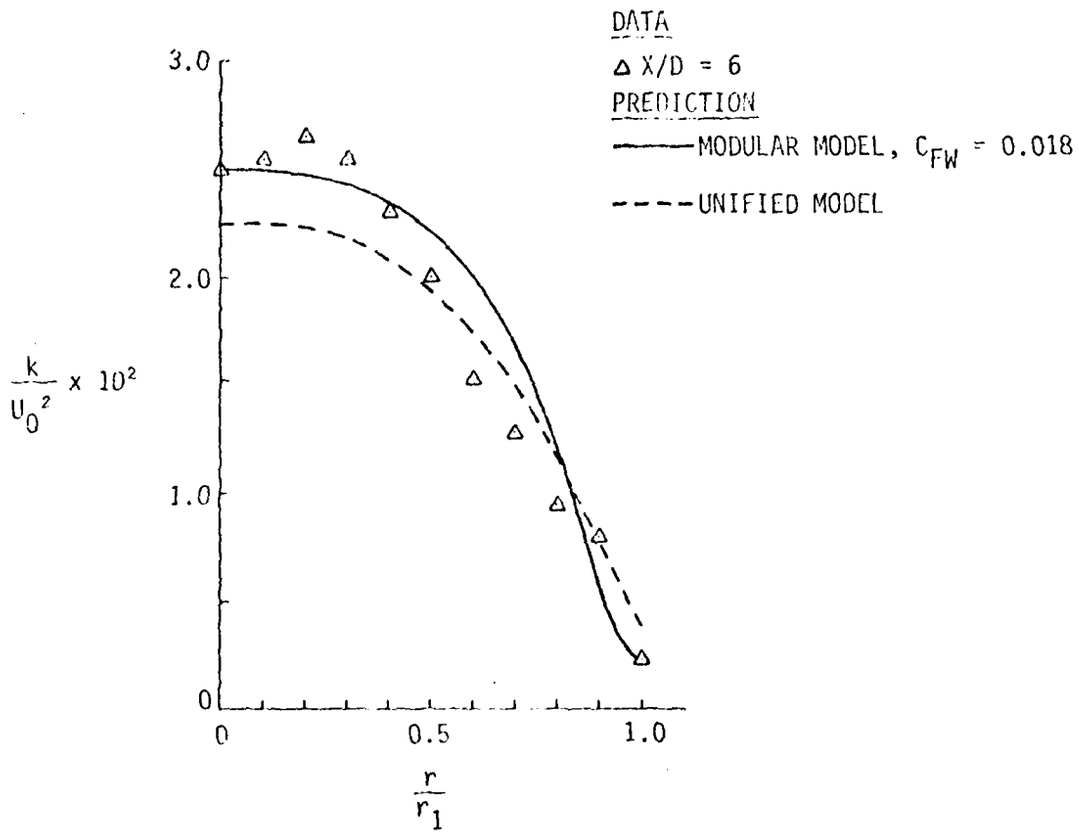

Figure 12. COMPARISON OF TURBULENT KINETIC ENERGY PROFILES PREDICTED BY MODULAR AND UNIFIED MODELS WITH DATA OF CHATURVEDI [15]

The configuration used experimentally by Craig, et al. [18] is, while still a sudden-expansion, considerably different from that studied by Chaturvedi [15]. The basic configuration studied in reference 18 involved a combustor L/D of 3, a dump area ratio A_3/A_2 of 2.25, and an exit nozzle area ratio A_2/A_3 = 0.40. Thus it is considerably shorter than Chaturvedi's apparatus, which had an L/D of 13 based on the "combustor" diameter, and incorporates an exit nozzle contraction which was not used in Chaturvedi's work. Both of these differences can be expected to have

substantial effects on the overall flowfield development. Two sets of inlet airflow rates and inlet total temperatures were used throughout the work reported in reference 18, with nominal values of 1.45 kg/sec and 0.73 kg/sec, and 555°K and 722°K, respectively. A major contribution of this work is the measurement of wall static pressure distributions in both cold flow and reacting flow. This report represents one of the few investigations in which these data, crucial to the comparison of experimental data with analytical model results, have been reported. Supplementing the results reported in reference 18, additional unreported static pressure distributions have been made available to the authors by Dr. Craig.

Although an appropriate set of model coefficients have been developed for Chaturvedi's configuration, the differences between that apparatus and the combustor used by Craig, et al. are substantial. Thus it can be expected that different parameter values would be necessary to accurately characterize Craig's combustor flowfield. In order to establish the necessary values, parametric calculations of one set of cold flow data, for an inlet total temperature of 552°K and an air mass flow of 1.45 kg/sec, were carried out. Figure 13 illustrates the results of these computations. Here, a parabolic recirculation zone shape was used, and those model parameters not noted on Figure 13 retained the values that were arrived at in the course of the computations of Chaturvedi's configuration. The inlet turbulent kinetic energy level and dissipation rate were established using the same relationships to mean flow and geometric variables as were used in the Chaturvedi calculations.

The differences in model parameters between the Chaturvedi [15] and Craig, et al. [18] cold flow configurations are the shape of the recirculation zone and the level of the dividing streamline shear stress coefficient. Although the comparisons shown in Figure 13 may indicate that a slight further refinement to the parabolic shape used in these calculations could improve the match between the computed and measured pressures over the range $0.5 < X/D < 1.5$, overall the level of agreement is quite good. The apparent lack of a large transition region between shear layer and wall boundary layer implied by these results, obtained

with no transition region, may be a result of the use of a converging exit nozzle in the Craig, et al. configuration. A further difference between the Craig, et al. configuration and that studied by Chaturvedi is the lack of an inlet section upstream of the dump plane in the latter case, compared to the use of a relatively long inlet section in the former. These computations use a uniform inlet profile so that the existence of an inlet boundary layer is reflected primarily in the shear stress parameter C_{FW}. Thus the requirement that the skin friction coefficient along the dividing streamline be a factor of 3 higher for the Craig, et al. comparison than for the Chaturvedi modeling may be a result of the differences in the initial conditions between the two flows.

CURVE	C_{FW}	b
A	0.018	0.05
B	0.040	0.05
C	0.050	0.09
D	0.055	0.09

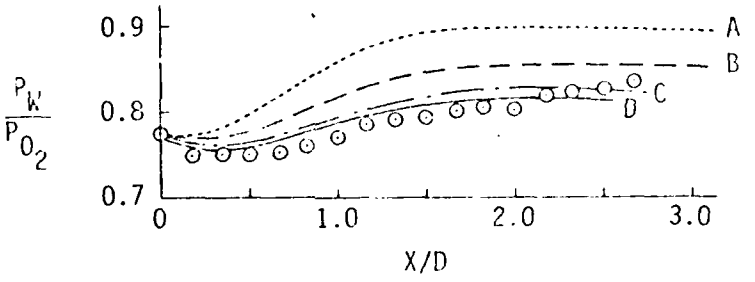

Figure 13. COMPARISON OF PREDICTED WALL STATIC PRESSURE DISTRIBUTIONS WITH COLD FLOW SUDDEN-EXPANSION COMBUSTOR DATA [18]

3.2 REACTING FLOW APPLICATIONS

Craig, et al. [18] also report combustion efficiency and wall static pressure distribution measurements for a premixed sudden expansion combustor. The combustor configuration is identical to that used in the cold flow investigation. To further test the modular model formulation, computations were made of a premixed dump combustor at a fuel-air ratio

of 0.053 for comparison with the data presented in reference 18. In the experiments, the fuel used was JP-4 which was represented in the computations by propane. Both a simple one-step global finite rate chemistry model and the full hydrocarbon oxidation kinetics as represented by the quasiglobal model [6, 19] were used to represent the chemical kinetics processes in the directed flow. The global model was used for the recirculation zone in both cases. Propane was chosen to represent the fuel because previous studies with propane had resulted in the development of a one-step finite rate kinetics model that represented fairly accurately the ignition delay for propane-air (although not the overall reaction time) over a range of conditions of interest in this work.

Initial conditions included an inlet total temperature of 554^{o}K (997^{o}R) and an inlet static pressure of 1.83 atm (3881 lb/ft^2). With a mass flow rate of 1.57 kg/sec (3.45 lb/sec), the inlet velocity and static temperature were 159 m/sec (521 ft/sec) and 543^{o}K (977^{o}R), respectively; the inlet Mach number was 0.351. Initial turbulent kinetic energy and dissipation rate values were established in the same manner as for the cold flow calculations, and the geometry of the combustor and recirculation zone was the same as in the cold flow calculations.

Both combustion efficiency and wall static pressure distribution data are available for this configuration, and the results of the modular model calculation of these quantities are shown in comparison with the experimental data in Figure 14. The combustion efficiency shown was computed from the mass-average temperature at each axial location in the calculation, using the JANNAF temperature-rise combustion efficiency definition, reference 20*. The "ideal" exit total temperature required for this calculation was obtained from the data tabulations provided to the authors by Dr. R. R. Craig of AFAPL; for these data, T_{T5}(ideal) = 2178^{o}K. Note that in these comparisons, data points are shown for the fuel/air ratio 0.053 value at which the computations were carried out. These data points were obtained from plotted values of combustion efficiency vs. fuel-air ratio presented in reference 18 for three different

* The definition was modified slightly in that static rather than total temperatures were used, for convenience. At the combustor Mach numbers encountered in these experiments, the difference in temperatures is of the order of 1 .

values of combustor L/D. The band shown for each data point represents the range of observed combustion efficiencies as a function of fuel-air ratio and is a better indication of the overall trend of the combustion efficiency vs. fuel-air ratio data than are the individual data points themselves. Some caution is advised in interpreting the combustion efficiency comparison shown in Figure 14 since three different combustor configurations were involved in obtaining the data. Thus the relationship between recirculation zone length and combustor length is different for each of the three combustors tested. On the other hand, the static pressure data (for two fuel-air ratios which bracket the fuel-air ratio used in the computation) and the predictions are both for a combustor L/D of 3.0.

The first point that should be noted in reviewing the results presented in Figure 14 is that the level of agreement with the data obtained was arrived at by increasing the kinetic energy level in the recirculation zone substantially over the levels found to be appropriate for the cold flow cases already discussed. One possible physical cause for this increased turbulent energy level in the recirculation region is the large-scale oscillation of the recirculation zone that has been observed in a variety of reacting, recirculating flowfields [19]. While the fluctuations that such oscillations produce are not strictly turbulence, two factors combine to suggest that they can be interpreted in the context of an analytical flow model as increased turbulent intensity levels in the recirculation zone. One is that the oscillations enhance the rate of mixing in the recirculation region and in the shear layer bounding it, and the second is that some of the energy in these oscillations can be expected to provide a source of turbulence energy. For all other factors equal, the increase in turbulent kinetic energy in the model recirculation zone, while not increasing the mixing rate within that region, does increase the effective viscosity along the dividing streamline, and thus the rate of transport across the shear layer. It also changes, both directly and indirectly through the transport mechanism, the rate of transport of turbulent kinetic energy to the recirculation zone. Thus the increased turbulent energy level in the recirculation

zone required to achieve good agreement with the available data for the Craig, et al. premixed combustor appears to be plausible on physical grounds.

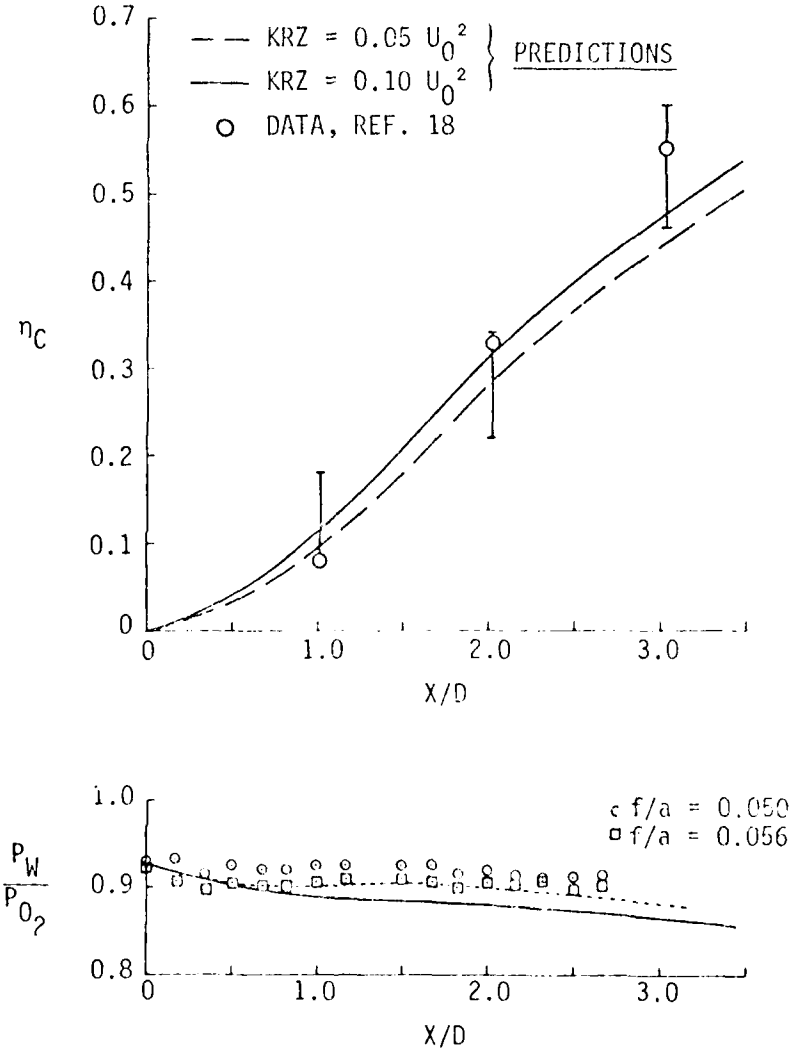

Figure 14. COMPARISON OF PREDICTED AND MEASURED COMBUSTION EFFICIENCY AND WALL STATIC PRESSURE DISTRIBUTIONS, PREMIXED SUDDEN-EXPANSION COMBUSTOR GLOBAL FINITE RATE CHEMISTRY MODEL

It is also of interest to note, from Figure 14, that the lower of the two curves shown in the combustion efficiency comparison provides the better agreement with the observed static pressure profiles, despite the significant underprediction by this computation of the combustion efficiency at X/D = 3.0. As has already been noted, the global finite rate model does not properly predict reaction time for the propane-air system used to model this flow, and thus further computations were carried out using the quasiglobal hydrocarbon kinetics model [6, 19] for the same conditions.

The initial quasiglobal computation of this flowfield, denoted by F = 1 on Figure 15, produced a surprising result: blowout was predicted to occur in the directed flow. To interpret this result, a digression to a discussion of the development of the quasiglobal chemical kinetics model for hydrocarbon oxidation is required.

During the development of the quasiglobal model, two major sources of data were utilized. One of these was ignition delay data obtained in experimental configurations approximating the ideal limit of plug flow, and the other was blowout data obtained from laboratory well-stirred reactors. Although data from both sources verified the basic quasiglobal model concept: that hydrocarbons higher than propane could be grouped into generic classifications and that for each group an overall partial oxidation reaction to the products CO and H_2 could be written, at least for fuel-air equivalence ratios less than one, it was observed that the effective pre-exponential coefficient in the quasiglobal Ahrrenius rate expression had to be increased by a factor of 80 for well-stirred reactor flows compared to plug flow.

The salient difference between a well-stirred reactor and a plug flow is that in the former the reactants and products of combustion are continuously being mixed with fresh, unreacted, entering species. This, of course, is the situation for a mixing and reacting flow, and it is expected to be particularly significant near blowout. Thus, a further series of computations were carried out with a multiplicative factor F preceding the pre-exponential coefficient in the quasiglobal hydrocarbon

partial oxidation rate expression [19]. For propane, this expression is

$$k_f = 6.0 \times 10^4 \, T \exp(-12{,}285/T) \qquad (42)$$

and values of F from the plug flow limit of 1 to the stirred reactor limit of 80 were considered. The rationale for carrying out this investigation is that each element of reacting fluid can be considered to behave as a combination of plug flow and stirred reactor flow: in the absence of turbulent transport each element is a plug flow reactor, whereas if turbulent transport dominates then the flow in each element approaches that of a homogeneous stirred reactor. This idealization is of course an oversimplification but it is an instructive concept.

As is shown in Figure 15, the well-stirred reactor limit, F = 80, drastically overpredicts the rate of reaction in comparison with the data, while for F = 5, blowout is still predicted. When F = 10 is selected, an almost perfect representation of the data is obtained, but this should be considered to be fortuitous: no representation that F = 10 is the appropriate value for mixing flows can or should be made.

If the predicted pressure profiles are considered, Figure 15, an entirely different conclusion could be obtained. Examination of these predictions shows that, while none of the predictions is in exact correspondence with the data, the predictions for F = 1 and F = 5 are in better agreement than those for F = 10 and F = 80. Significantly, the disagreement in the latter two cases is greatest in the region downstream of the end of the recirculation zone for this configuration, and is thus not related to the dividing streamline modeling incorporated in the model approach. The data presented by Craig, et al. [18] indicate that for the premixed combustor, blowout is observed between a fuel-air ratio of 0.030 and 0.040. The sensitivity of these results to the parameter F, observed in Figure 15, is an indication that at the conditions of these data, a fuel-air ratio of 0.053, the flowfield is also near blowout. In fact, the combination of the agreement with the axial pressure profiles obtained for F = 1 and F = 5 and the agreement with the measured combustion efficiency for F = 10 can be taken to indicate that this combustor flow was,

in fact, oscillatory, with a continuous partial blowout and reignition phenomena occurring during the test.

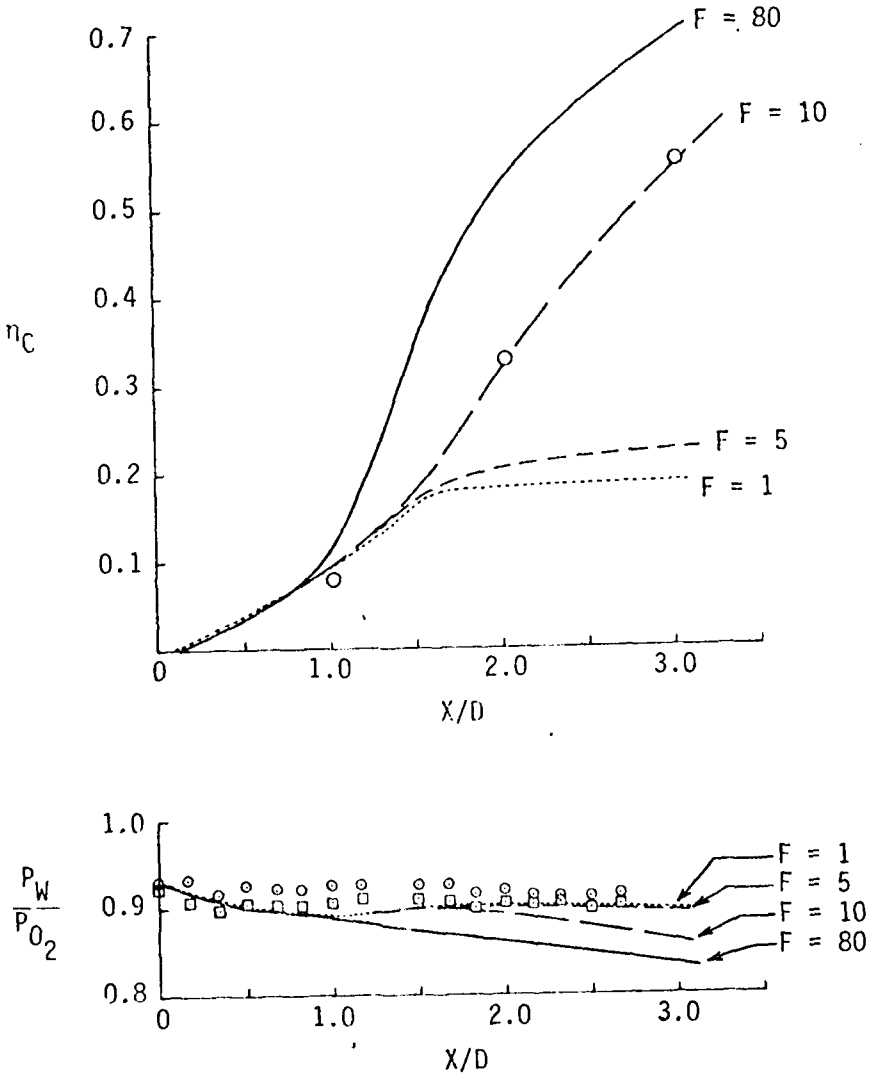

Figure 15. COMPARISON OF PREDICTED AND MEASURED COMBUSTION EFFICIENCY AND WALL STATIC PRESSURE DISTRIBUTIONS; DATA FROM CRAIG, et al. [18]

This discussion has emphasized the model sensitivities observed during this phase of the model validation program. It is, of course, also instructive to consider the insensitivities observed. These can be summarized as follows:

- For the premixed reacting flow, the predictions are insensitive to the details of the shear layer growth rate, as modeled by Eq. 29.
- The premixed combustor is totally insensitive to initial velocity profile variation as represented by the inclusion in the initial profile of a 1/7 power law boundary layer with a thickness equal to 0.1 times the inlet radius.

SECTION 4
APPLICATION OF UNIT ANALYSES TO COMBUSTOR PROBLEMS

Although this report has focused on the application of the complete modular model to the analysis and interpretation of combustor data, unit analyses can also provide considerable insight into various aspects of combuster performance. These unit analyses can themselves be elements of an overall modular combustor model: one of the advantages of modular modeling is that the model elements can be individually developed and verified through use as unit analysis tools. In this section, two types of unit analyses will be discussed. The first example involves the use of a simple droplet vaporization analysis to interpret experimental data in a laboratory combustor, while the second example involves the use of the well-stirred reactor module of the modular model as a unit analysis of flameholder blowout phenomena.

4.1 DROPLET VAPORIZATION EFFECTS ON COMBUSTOR PERFORMANCE

Because of the requirement for greater energy density than conventional fuels, ramjet fuels can have considerably different physical characteristics from fuels such as JP-4. These physical characteristics include viscosity, which is generally greater for ramjet fuels, and volatility, which is in general lower. These differences can be expected to lead to larger and more persistent fuel droplets for ramjet fuels than for conventional fuels.

The combustion characteristics of several ramjet fuels were investigated by Siminski [21], who presented data for the specific impulse (ISP) efficiency obtained using various fuels in a simulated ramjet combustor. These data show a strong dependence of η_{ISP} on inlet temperature for low inlet temperatures. The fuel was injected into the combustor in liquid form, so that the vaporization rate of the fuel can be expected to have an impact on the overall combustor performance. Since η_{ISP} is related to the actual total temperature rise in the combustion

process divided by the ideal total temperature rise, and this can in turn be related to the vapor fuel concentration divided by the initial liquid fuel concentration, which in turn is directly relatable to the fuel vaporization rate, a relation between η_{ISP} and vaporization rate can be devised:

$$\eta_{ISP} \propto \left(\frac{T_0 \text{ actual}}{T_0 \text{ ideal}}\right)^{\frac{1}{2}} \simeq \left(\frac{\alpha_v}{\alpha_{F,0}}\right)^{\frac{1}{2}}$$

and

$$\frac{\alpha_v}{\alpha_{F,0}} = 1 - \left(\frac{d}{d_0}\right)^3$$

so

$$\eta_{ISP} \propto \left[1 - \left(\frac{d}{d_0}\right)^3\right]^{\frac{1}{2}} \tag{43}$$

This correlation was tested by computing vaporization rates as a function of gas-droplet ΔT for two droplet sizes and for two fuels, RJ-5 and JP-5, which differ substantially in viscosity and boiling point temperature. A simple one-dimensional droplet vaporization computation was used, incorporating the "d^2" vaporization law

$$d^2 = d_0^2 - \lambda \frac{Nu}{2} t \tag{44}$$

where Nu is the Nusselt number and λ is an evaporation rate constant which depends on droplet thermal conductivity, density, specific heat and heat of vaporization and on the droplet-gas phase temperature difference. The solution for droplet diameter, d, is obtained through use of the "d^2" law coupled to one-dimensional statements of momentum and energy transport for the droplet exposed to a uniform gas-phase environment. Droplet diameter was computed at a time from injection corresponding approximately to the time required for the fuel to reach the flameholder in the combustor used by Siminski [21]. The agreement between the correlation and the data is striking for both fuels, as shown in Figures 16

and 17. Since the droplet size in the apparatus used by Siminski was not known, a range of sizes was used; it might be expected that at similar conditions the RJ-5 would form larger droplets than the JP-5 because of its higher viscosity. Note also from Figure 16 that the agreement of the correlation for smaller droplets with the data at the higher fuel temperature is consistent with a reduction in drop size with fuel temperature increase (due to a fuel viscosity increase); this is also seen for JP-5, Figure 17 for the lower ΔT (and therefore higher fuel temperature) range.

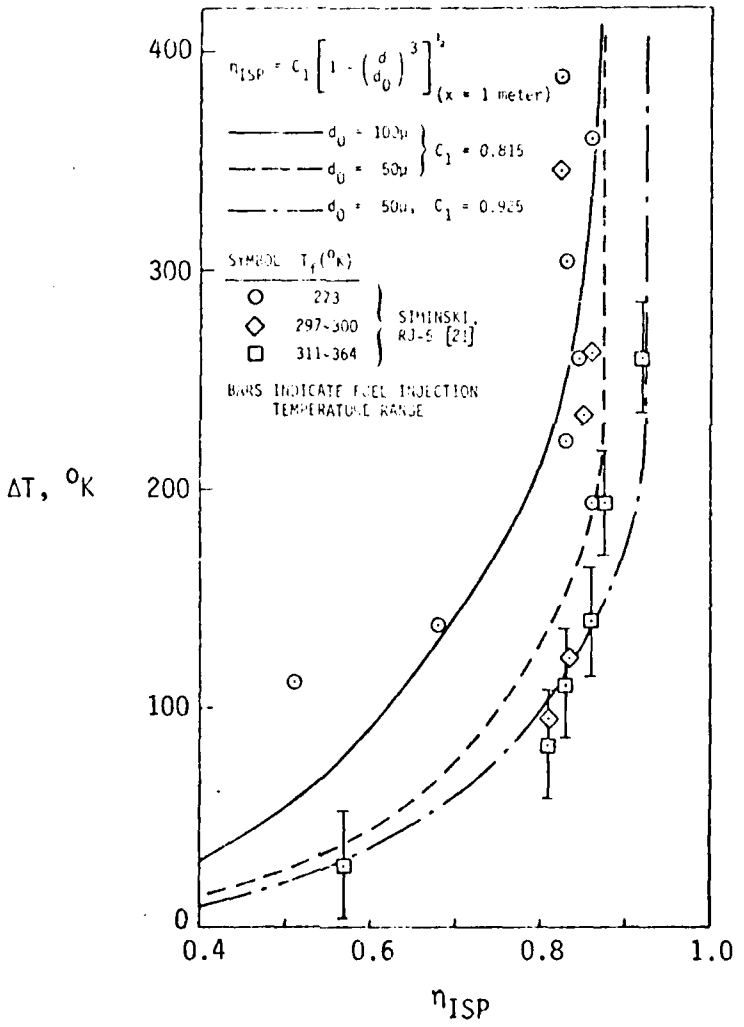

Figure 16. CORRELATION BETWEEN VAPORIZATION RATE AND ISP EFFICIENCY, RJ-5 FUEL

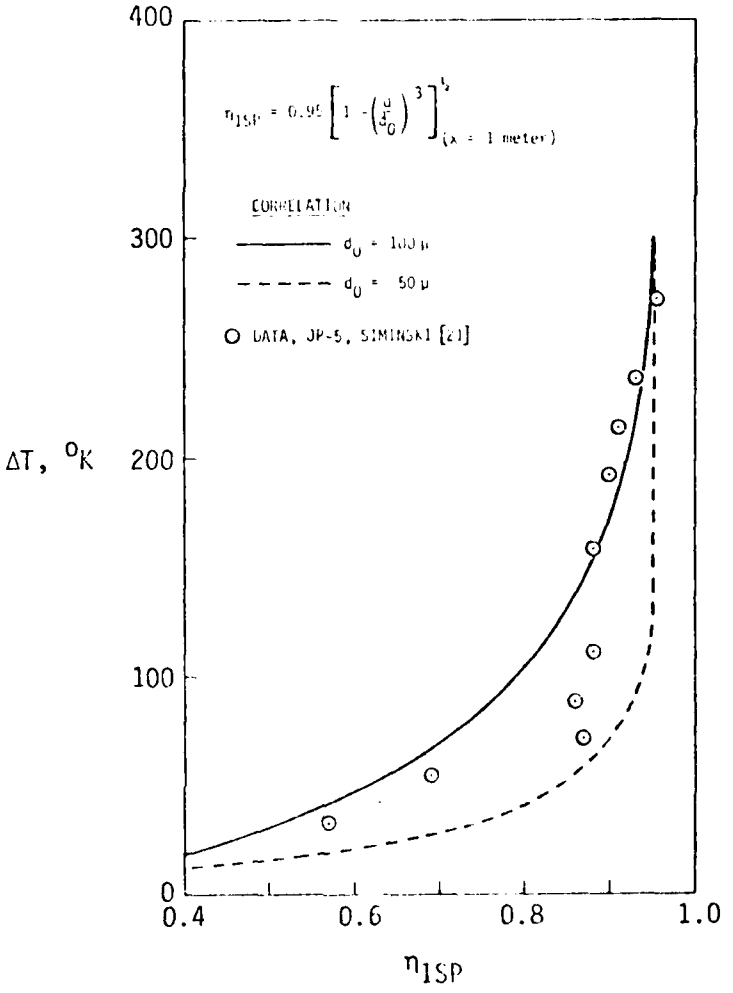

Figure 17. CORRELATION BETWEEN VAPORIZATION RATE AND ISP EFFICIENCY, JP-5 FUEL

4.2 FLAMEHOLDER BLOWOUT AT HIGH INLET TEMPERATURE

The well-stirred reactor analysis is a model of a laboratory well-stirred reactor. It is also a model of a recirculation region, such as that downstream of the dump station in a sudden-expansion combustor, or that behind a flameholder. Thus the well-stirred reactor model can be used as a unit analysis of flameholder flame stabilization phenomena.

An example of the use of the well-stirred reactor model in the study of flame stabilization phenomena is the study of the effects of vitiation on flameholder performance. In order to achieve high combustor inlet temperatures in a ramjet ground test facility, vitiation of the inlet air stream is often necessary, and even if a hydrocarbon fuel such as propane is used as the vitiator fuel, with oxygen makeup, serving to minimize potential molecular weight mismatch between the vitiated test stream and the inlet air stream at flight conditions, the question of the effects of vitiation on measured flameholder performance still arises. Flame stabilization can be modeled using the well-stirred reactor as an approximation to an intensely backmixed recirculation region behind a flameholder. The loading parameter for this well-stirred reactor at blowout then becomes a characterization of the flame stability which can be expected. To study the effects of vitiation on flame stabilization at high inlet temperatures, well-stirred reactor calculations were carried out, using both pure and vitiated air inlet streams.

Results of these computations are shown in Figure 18 for one test condition of interest. The effect of vitiation for these conditions can be seen to be a reduction of the loading parameter at blowoff, because of the effects of the presence of H_2O and CO_2 on the specific heat of the "air" mixture.

These results are presented in terms of a reduced loading parameter as used in Curran [22]; in general the reduced loading parameter is defined as

$$RLP = \frac{\dot{n}_A}{VP^{1.8}} \left(\frac{A}{T_i^b} \right) \tag{45}$$

with A and b designated as empirical parameters. In actuality, the exponent on the pressure is itself an empirical parameter. If the non-vitiated results shown in Figure 18 are considered, a comparison of these data with the available experimental results (from references 22, 23 and 19) indicates that, for a pressure exponent of 1.8, the temperature exponent

b varies from 1.0 at an equivalence ratio of 0.4 to 1.46 at an equivalence ratio of 1.0, as shown by the additional points on Figure 18. However, the data shown in Figure 18 were obtained at one atmosphere pressure, while the computations are for a pressure level of about two atmospheres. Thus the effects of the use of a pressure exponent of 1.8 are also included in these results. Further computations, at temperature and pressure levels that are elevated with respect to the available data, can serve to indicate the appropriate values for both the pressure and temperature exponents in Eq. 45.

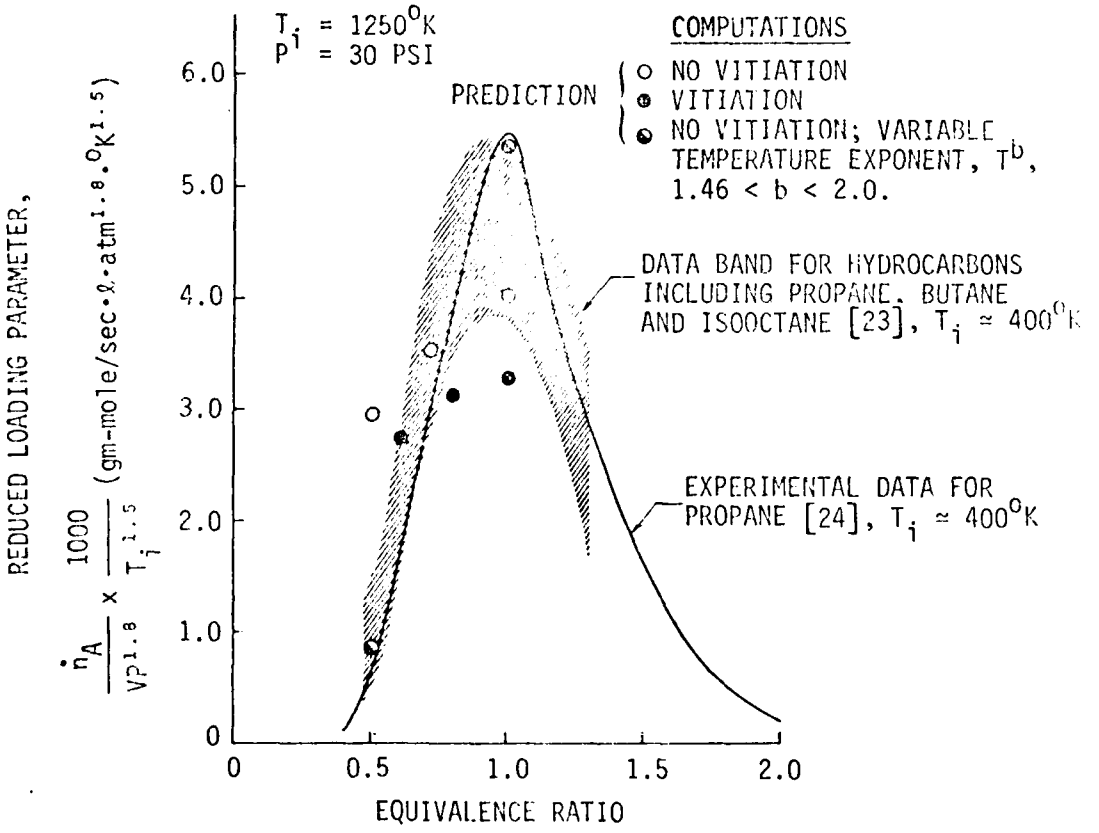

Figure 18. COMPARISON OF COMPUTED BLOWOUT RESULTS FOR HIGH TEMPERATURE CONDITIONS WITH EXPERIMENTAL STIRRED REACTOR DATA

SECTION 5 - CONCLUSIONS

While the computational ability to predict in detail the flowfield in a ramjet combustor without empirical approximations appears to remain a long-term goal rather than a short-term prospect, modeling techniques have been shown to be a viable tool in the analysis of ramjet combustion processes. These modeling techniques range from the analysis of plug flow and well-stirred reactor flows, which represent idealizations of aspects of an overall ramjet flowfield, to the modular approach, which represents the only realistic method of introducing a detailed description of a ramjet combustor flowfield into a computational technique.

The modular approach is not a predictive technique, and no currently available mathematical model of a ramjet combustor can be considered to be truly predictive. What the modular approach, coupled with the use of detailed unit analyses offers, is the ability to analyze and interpret experimental data and to aid in the design and planning of appropriate experiments.

A considerable amount of further work is still required to develop all viable ramjet modeling approaches, whether unified or modular formulations. What the work described in this report has shown is the insight that can be gained through the use of modeling in both the design of combustors and experiments and in the interpretation of experimental results. It is in this area that modeling holds the greatest promise.

REFERENCES

1. Hutchinson, P., Khalil, E. E., and Whitelaw, J. H., "Measurement and Calculation of Furnace-Flow Properties," Journal of Energy, Vol. 1, No. 4, July-August 1977, pp. 212-219.

2. Abou Ellail, M. M. M., Gosman, A. D., Lockwood, F. C., and Megahead, I. E. A., "Description and Validation of a Three-Dimensional Procedure for Combustion Chamber Flows," Report FS/77/27, Imperial College, Oct. 1977.

3. Roberts, R. A., Aceto, L. D., Kollrack, R., Teixeira, D. P., and Bonnell, J. M., "An Analytical Model for Nitric Oxide Formation in a Gas Turbine Combustor," AIAA Journal, Vol. 10, No. 6, June 1972.

4. Swithenbank, J., Poll, I., Vincent, M. W., and Wright, D. D., "Combustion Design Fundamentals," Fourteenth Symposium (International) on Combustion, The Combustion Institute, Pittsburgh, 1973, pp. 627-636.

5. Harsha, P. T. and Edelman, R. B., "Application of Modular Modeling to Ramjet Performance Prediction," AIAA Paper 78-944, Fourteenth Joint Propulsion Conference, Las Vegas, Nevada, July 25-27, 1978.

6. Edelman, R. B. and Fortune, O., "A Quasi-Global Chemical Kinetic Model for the Finite Rate Combustion of Hydrocarbon Fuels," AIAA Paper 69-86, 1969.

7. Launder, B. E., Morse, A., Rodi, W., and Spalding, D. B., "Prediction of Free Shear Flows - A Comparison of the Performance of Six Turbulence Models," in Free Turbulent Shear Flows, Vol. I, Conference Proceedings, NASA Report No. SP-321, 1973, pp. 463-519.

8. Boccio, J. L., Weilerstein, G., and Edelman, R. B., "A Mathematical Model for Jet Engine Combustor Pollutant Emissions," NASA CR-121088, GASL TR-781, General Applied Science Laboratories.

9. Edelman, R. B. and Weilerstein, G., unpublished work, 1971.

10. Prandtl, L., "Bemerkungen zur Theorie der Freien Turbulenz," Zeitschrift fur Angewandte Mathematik und Mechanik, Vol. 22, 1942, pp. 241-243.

11. Harsha, P. T., Free Turbulent Mixing: A Critical Evaluation of Theory and Experiment, Arnold Engineering Development Center, AEDC TR-71-36, 1971.

12. Catton, I., Mill, [illegible] Rao, R. D., "[illegible] Liquid Jet Penetration in [illegible] Stream," AI[illegible], No. 11, November 1[illegible].

13. Clark, B., "Breakup of a Liquid Jet in [illegible] Flow of Gas," NASA TN-D-2424, August 1964.

14. Ingebo, R. and Foster, H., "Drop Size Distribution for Cross-Current Break-up of Liquid Jets in Air Stream," NACA [illegible], October 1957.

15. Chaturvedi, M. C., "Flow Characteristics of Axisymmetric Expansions," Journal of the Hydraulics Division, Proceedings of the American Society of Civil Engineers, Vol. 89, No. [illegible], May 1963, pp. 61-92.

16. Drewry, James E., "Characterization of Sudden-Expansion Dump Combustor Flowfields," AFAPL-TR-76-52, Air Force Aero Propulsion Laboratory, July 1976.

17. Turan, Ali, PhD Thesis, University of Sheffield, 1979.

18. Craig, R. R., Drewry, J. E., and Stull, F. D., "Coaxial Dump Combustor Investigation," AIAA Paper 78-1107, AIAA/SAE 14th Joint Propulsion Conference, July 25-27, 1978.

19. Edelman, R. B. and Harsha, P. T., "Laminar and Turbulent Gas Dynamics in Combustors - Current Status," Progress in Energy and Combustion Science, Vol 4, No. 1, 1978, pp. 1-62.

20. Airbreathing Combustor Development Committee, "Recommended Ramburner Test Reporting Standards," CPIA Publication 276, Chemical Propulsion Information Agency, March 1976.

21. Siminski, V. J., "Hydrocarbon Fuel Study Program - Final Technical Report," NWC TP 5468, Naval Weapons Center, China Lake, CA, 1975.

22. Curran, E. T., "An Investigation of Flame Stability in a Coaxial Dump Combustor," PhD Thesis, Air Force Institute of Technology, 1979.

23. Edelman, R. B. and Weilerstein, G., "A Theoretical Study of Combustion and NO Formation in Well-Mixed Regions," Technical Report 758, General Applied Science Laboratories, May 1971.

24. Ernst, R. C., "Flameholder Combustion Instability Study," Report AFAPL-TR-78-24, Air Force Aero Propulsion Laboratory, May 1978.

APPENDIX I
NUMERICAL SOLUTION TECHNIQUE FOR DIRECTED FLOW ANALYSIS

The solution technique used for the directed flow portion of the modular model involves the use of a Von-Mises type transformation of the governing equations to a stream function coordinate system and an explicit finite-difference solution of the resulting equations. To illustrate the technique, consider the axial momentum equation; which, for axisymmetric flow, in boundary layer form, can be written

$$\rho u \frac{\partial u}{\partial x} + \rho v \frac{\partial v}{\partial r} = \frac{1}{r} \frac{\partial}{\partial r} \left\{ \rho \nu_T r \frac{\partial u}{\partial r} \right\} - \frac{\partial p}{\partial x} \tag{I-1}$$

Using the transformation

$$\psi \, d\psi = \rho u r \, dr \tag{I-2}$$

at constant x, Eq. I-1 becomes

$$\frac{\partial u}{\partial x} = \frac{1}{\psi} \frac{\partial}{\partial \psi} \left\{ \frac{\rho^2 u \nu_T r^2}{\psi} \frac{\partial u}{\partial \psi} \right\} - \frac{1}{\rho u} \frac{\partial p}{\partial x} \tag{I-3}$$

This equation is valid throughout the flowfield except on a centerline where both r and ψ become zero. However, the limiting form of Eq. I-3 for the centerline can be obtained through use of L'Hospital's rule, yielding

$$\left. \frac{\partial u}{\partial x} \right|_{\substack{\psi=0 \\ r=0}} = 2 \rho \nu_T \frac{\partial^2 u}{\partial \psi^2} - \frac{1}{\rho u} \frac{\partial p}{\partial x} \tag{I-4}$$

Similar transformation and limiting form behavior applies to the other governing equations in the flow.

The governing partial differential equations describing the conservation of mass, momentum, and energy within the flowfield and along the axis can be readily put in an explicit finite-difference form. A backward-difference scheme is employed for the axial derivatives and a central-difference scheme for the radial derivatives.

Consider the flowfield divided into a grid in ψ, x coordinates. Then the derivatives of an independent variable, say F, will be evaluated by

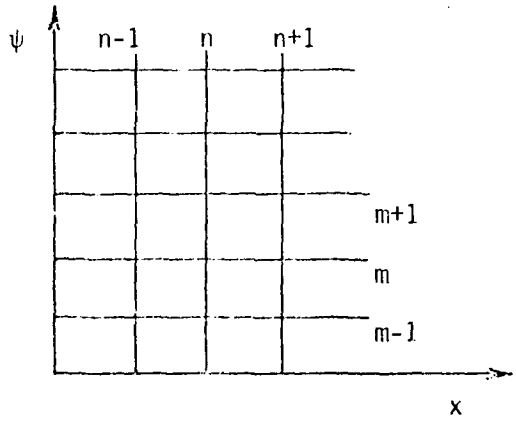

$$\left(\frac{\partial F}{\partial x}\right)_{n+1,m} = \frac{F_{n+1,m} - F_{n,m}}{\Delta x} = \frac{\Delta(F)_{n+1,m}}{\Delta x} \tag{I-5}$$

$$\left(\frac{\partial F}{\partial \psi}\right)_{n,m} = \frac{F_{n,m+1} - F_{n,m-1}}{2\Delta\psi} \tag{I-6}$$

$$\left[\frac{\partial}{\partial \psi}\left(a\,\frac{\partial F}{\partial \psi}\right)\right]_{n,m} = \frac{a_{n,m+\frac{1}{2}}\,(F_{n,m+1} - F_{n,m}) + a_{n,m-\frac{1}{2}}\,(F_{n,m-1} - F_{n,m})}{(\Delta\psi)^2} \tag{I-7}$$

where

$$a_{n,m\pm\frac{1}{2}} = (a_{n,m} + a_{n,m\pm1})/2 \tag{I-8}$$

and

$$\frac{\partial^2 F}{\partial \psi^2}_{n,m} = \frac{F_{n,m+1} - 2F_{n,m} + F_{n,m-1}}{(\Delta\psi)^2} \tag{I-9}$$


DAT
FILM